Mixed finite element methods: implementation with one unknown per element, local flux expressions, positivity, polygonal meshes, and relations to other methods [*]

Martin Vohralík[1] and Barbara Wohlmuth[2]

[1]UPMC Univ. Paris 06, UMR 7598, Laboratoire Jacques-Louis Lions, 75005, Paris, France
&
CNRS, UMR 7598, Laboratoire Jacques-Louis Lions, 75005, Paris, France
e-mail: vohralik@ann.jussieu.fr

[2] Fakultät für Mathematik, Lehrstuhl für Numerische Mathematik
Boltzmannstrasse 3, 85748 Garching bei München, Germany
e-mail: wohlmuth@ma.tum.de

Abstract

In this paper, we study the mixed finite element method. We focus on the lowest-order Raviart–Thomas case and propose several new ways of reducing the original indefinite saddle-point systems for flux and potential unknowns to (positive definite) systems for potential unknowns only. It turns out that the principle of our construction is closely related to that of the so-called multi-point flux-approximation method. We study theoretically these different ways and illustrate them by a series of numerical test examples. We also discuss the different versions of the discrete maximum principle and of obtaining local flux expressions in the mixed finite element method. We finally recall the use of the mixed finite element method on general polygonal meshes and expose its similarity to mimetic finite difference, multi-point flux-approximation, mixed finite volume, and hybrid finite volume methods in this case.

Key words: mixed finite element method, reformulation, one unknown per element, local flux expression, discrete maximum principle, polygonal mesh, relations between different methods

1 Introduction

We consider in this paper the pure diffusion model problem

$$-\nabla \cdot (\mathbf{S}\nabla p) = g \qquad \text{in } \Omega, \tag{1.1a}$$

$$p = 0 \qquad \text{on } \partial\Omega, \tag{1.1b}$$

where $\Omega \subset \mathbb{R}^d$, $d \geq 2$, is a polygonal (we use this term also in $\mathbb{R}^d$, $d \geq 3$) domain. The system (1.1a)–(1.1b) will be discretized on a family of meshes $\mathcal{T}_h$ of Ω, consisting of simplices and

matching (containing no "hanging nodes"); we refer to Section 2 below for the details on terminology and notation. For simplicity, we restrict ourselves to homogeneous Dirichlet boundary conditions and assume that $\mathbf{S}$ is a symmetric, bounded, and uniformly positive definite diffusion tensor, piecewise constant on $\mathcal{T}_h$. Similarly, we assume that g is piecewise constant on $\mathcal{T}_h$. A wider class of meshes $\widehat{\mathcal{T}}_H$, consisting of general polygonal elements, will also be considered later.

We are interested in mixed finite element approximations to (1.1a)–(1.1b). These consist in finding $p_h \in \Phi_h$, an approximation to the *potential* p, and $\mathbf{u}_h \in \mathbf{V}_h$, an approximation to the *flux* $\mathbf{u} := -\mathbf{S}\nabla p$, such that

$$(\mathbf{S}^{-1}\mathbf{u}_h, \mathbf{v}_h) - (p_h, \nabla \cdot \mathbf{v}_h) = 0 \qquad \forall \mathbf{v}_h \in \mathbf{V}_h, \tag{1.2a}$$

$$(\nabla \cdot \mathbf{u}_h, \phi_h) = (g, \phi_h) \qquad \forall \phi_h \in \Phi_h. \tag{1.2b}$$

Here $\Phi_h \subset L^2(\Omega)$ and $\mathbf{V}_h \subset \mathbf{H}(\mathrm{div}, \Omega)$ are the mixed finite element spaces (cf. Brezzi and Fortin [19] or Roberts and Thomas [58]). We focus here on the lowest-order Raviart–Thomas case, where Φ_h consists of piecewise constant functions on $\mathcal{T}_h$ and $\mathbf{V}_h$ is recalled in Section 3 below. The system (1.2a)–(1.2b) can be written in a matrix form as

$$\begin{pmatrix} \mathbb{A} & \mathbb{B}^t \\ \mathbb{B} & 0 \end{pmatrix} \begin{pmatrix} U \\ P \end{pmatrix} = \begin{pmatrix} F \\ G \end{pmatrix} \tag{1.3}$$

and is of *indefinite, saddle point* type. In our case, thanks to the homogeneous Dirichlet boundary condition (1.1b), $F = 0$, but we prefer to write the general form (1.3) with F not necessarily zero. The system (1.3) is *well-posed*; $\mathbb{A}$ is symmetric and positive definite and $\mathbb{B}$ has a full row rank. Thus, there exists a unique solution, on any simplicial mesh $\mathcal{T}_h$, without any restriction on the shape of the elements; the usual shape-regularity of the mesh is only necessary in convergence proofs. Recall also that the system (1.3) is well-posed in any space dimension. All these classical results can be found in, e.g., [19, 58, 66].

Let $\sigma_{K,L} \in \mathcal{E}_h^{\mathrm{int}}$, i.e., $\sigma_{K,L}$ is an interior side of the mesh $\mathcal{T}_h$, shared by the elements K and L. The approximate fluxes $\mathbf{u}_h$ of (1.2a)–(1.2b) satisfy $\mathbf{u}_h|_K \cdot \mathbf{n}_{\sigma_{K,L}} = \mathbf{u}_h|_L \cdot \mathbf{n}_{\sigma_{K,L}}$, where $\mathbf{n}_{\sigma_{K,L}}$ is a normal vector of $\sigma_{K,L}$. This is a consequence of the constraint $\mathbf{V}_h \subset \mathbf{H}(\mathrm{div}, \Omega)$, also called the "normal trace continuity constraint", which ensures the conservation of mass. This constraint can be relaxed using the hybridization technique. Herein, it is imposed instead in terms of Lagrange multipliers. The unconstrained flux space is given by $\tilde{\mathbf{V}}_h := \Pi_{K \in \mathcal{T}_h} \mathbf{V}_h(K)$, where $\mathbf{V}_h(K)$ are the local spaces on each element (cf. Section 3 below), and the Lagrange multipliers space Ψ_h is the space of piecewise polynomials (constants in the lowest-order case) on $\mathcal{E}_h^{\mathrm{int}}$. The hybridized version of (1.2a)–(1.2b) consists in finding $\mathbf{u}_h \in \tilde{\mathbf{V}}_h$, $p_h \in \Phi_h$, and $\lambda_h \in \Psi_h$ such that

$$(\mathbf{S}^{-1}\mathbf{u}_h, \mathbf{v}_h) - (p_h, \nabla \cdot \mathbf{v}_h) + \sum_{K \in \mathcal{T}_h} \langle \mathbf{v}_h \cdot \mathbf{n}_K, \lambda_h \rangle_{\partial K \setminus \partial \Omega} = 0 \qquad \forall \mathbf{v}_h \in \tilde{\mathbf{V}}_h, \tag{1.4a}$$

$$(\nabla \cdot \mathbf{u}_h, \phi_h) = (g, \phi_h) \qquad \forall \phi_h \in \Phi_h, \tag{1.4b}$$

$$\sum_{K \in \mathcal{T}_h} \langle \mathbf{u}_h \cdot \mathbf{n}_K, \psi_h \rangle_{\partial K \setminus \partial \Omega} = 0 \qquad \forall \psi_h \in \Psi_h. \tag{1.4c}$$

It is well known and easy to show that $p_h, \mathbf{u}_h$ from (1.2a)–(1.2b) and (1.4a)–(1.4c) coincide; λ_h then provides an additional approximation to the potential p. The equations (1.4a)–(1.4c) can be written in a matrix form as

$$\begin{pmatrix} \mathbb{A} & \mathbb{B}^t & \mathbb{C}^t \\ \mathbb{B} & 0 & 0 \\ \mathbb{C} & 0 & 0 \end{pmatrix} \begin{pmatrix} U \\ P \\ \Lambda \end{pmatrix} = \begin{pmatrix} F \\ G \\ 0 \end{pmatrix}. \tag{1.5}$$
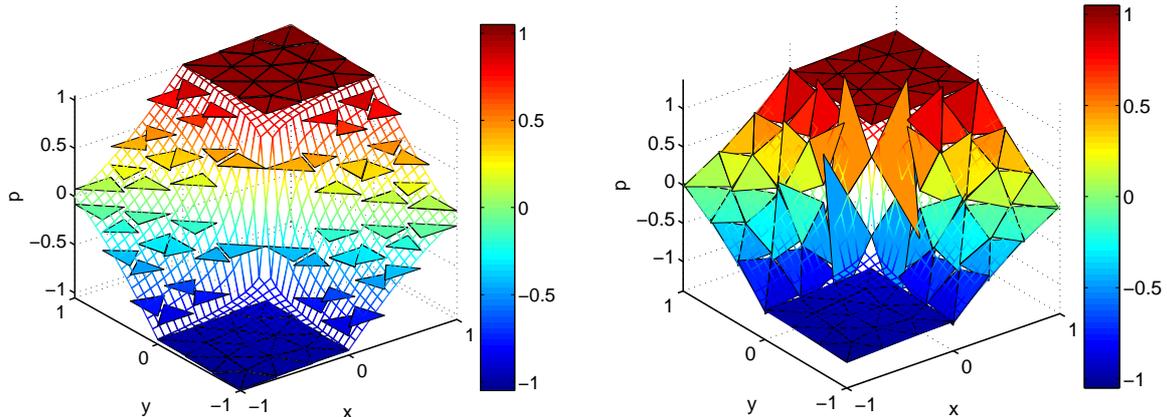
Figure 1: Mixed finite element potential represented by p_h (left) and by $\tilde{\lambda}_h$ (right)

The importance of the hybridization (1.5) lies in that the matrix $\mathbb{A}$ has now an elementwise block-diagonal structure. Consequently, one can algebraically, solving only *local problems* (inverting local matrices), reduce (1.5) to the system for the Lagrange multipliers Λ only,

$$\mathbb{Z}\Lambda = E. \tag{1.6}$$

Here $\mathbb{Z}$ is a *symmetric* and *positive definite matrix* with a *narrow stencil* (there are at most $2(d+1)-1$ nonzero entries on each row of $\mathbb{Z}$); closed-form expressions for $\mathbb{Z}$ and E are given in Section 3.1 below. Remark that the total number of unknowns is reduced in comparison with (1.3), being given by the number of sides in $\mathcal{E}_h^{\mathrm{int}}$. This process is called *static condensation*. We refer for details to [19, 58]. A new, piecewise affine nonconforming approximation $\tilde{\lambda}_h$ of the potential p, given by the values of λ_h in side barycenters (see (3.3) below) can also be defined. Such an approximation is visualized in Figure 1, right; we plot the corresponding approximation p_h in Figure 1, left.

There has been a long-standing interest to *reduce* (1.3) to a system for the *potentials P only*. The main motivations are to reduce the number of unknowns, to replace the saddle point system (1.3) by, if possible, a symmetric and positive definite one, and to relate the lowest-order mixed finite element method to the finite difference and finite volume ones. A possible solution consists in first using the first block equation of (1.3) to eliminate the unknowns U through

$$U = \mathbb{A}^{-1}(F - \mathbb{B}^t P). \tag{1.7}$$

Note that (1.7) represents a *global flux expression* (all the fluxes U are expressed from all the potentials P), which includes a solution of a global linear system. Plugging (1.7) into the second block equation of (1.3), one can solve for P the system

$$\mathbb{B}\mathbb{A}^{-1}\mathbb{B}^t P = \mathbb{B}\mathbb{A}^{-1}F - G. \tag{1.8}$$

The matrix $\mathbb{B}\mathbb{A}^{-1}\mathbb{B}^t$ is symmetric and positive definite but the problem is that it tends to be *full* and *cannot be obtained in practice* as this would be too expensive. Various approximate numerical quadratures have been used in, e.g., [59, 6, 14, 12, 10] to reduce (1.3) into a system of the form

$$\widetilde{\mathbb{S}}\widetilde{P} = \widetilde{H}. \tag{1.9}$$

In these approaches, however, because of the numerical quadratures, the *new potentials* $\widetilde{P}$ are in general *different* from those in (1.3) and one cannot recover the exact potentials P.
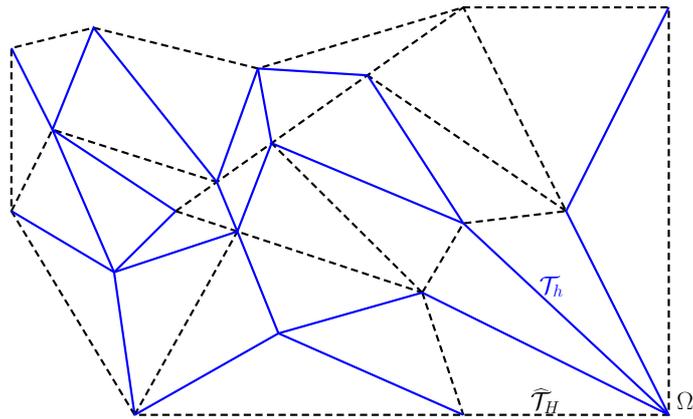
Figure 2: Example of a general polygonal mesh $\widehat{\mathcal{T}}_H$ (dashed lines) and of a possible simplicial submesh $\mathcal{T}_h$ (solid lines)

Equivalent, one-unknown-per-element rewriting of (1.3) *without any numerical quadrature* in the form

$$\bar{\mathbb{S}}\bar{P} = \bar{H}, \tag{1.10}$$

where $\bar{P}$ is a *new unknown* from which P can be *locally recovered*, has been achieved in [72, 24, 71] by exploiting an equivalence between mixed finite elements and finite volumes. Equivalent, one-unknown-per-element rewriting of (1.3) *without any numerical quadrature* in the form

$$\mathbb{S}P = H \tag{1.11}$$

has been derived in [64]. In both the above approaches, in contrast to (1.9), one obtains *exactly* the potentials P of (1.3) (there is no approximation included), and in contrast to (1.8), the matrices $\bar{\mathbb{S}}$ and $\mathbb{S}$ are *sparse* and *locally computable*. Intermediately, *local flux expressions* (enabling to recover the fluxes U of (1.3) on sides of local patches from the potentials P on elements of these patches) have been established in [72, 24, 71, 64]. For some alternative ways of reduction of the number of unknowns in (1.3), we refer to [8, 62] and the references therein.

The first goal of the present paper is to *unify the approaches* of [72, 24, 71] and of [64], to identify their common principles, and to show that they can be included in the general approach given in [70]. We tackle this issue in Section 4, after recalling some basic facts about the lowest-order Raviart–Thomas method in Section 3, and summarizing the notation in Section 2. In Section 3, we also recall the relation of the lowest-order Raviart–Thomas method to the Crouzeix–Raviart nonconforming finite element method, local flux expressions from the Lagrange multipliers, and the different variants of the discrete maximum principle valid in this case.

The second goal of the present paper is to carry out an *extensive comparative numerical study* of the different one-unknown-per-element lowest-order mixed finite element reformulations. We in particular focus on the behavior of the different approaches in the presence of inhomogeneous and anisotropic diffusion tensor **S**. We carry out this study in Section 6.

The third goal of the present paper is to recall that, contrarily to a widespread misleading belief, mixed finite elements can easily be defined on *general polygonal meshes*. We present this result in Section 5 for all order schemes on practically arbitrary meshes and without loosing any precision with respect to (1.2a)–(1.2b); we refer to Kuznetsov and Repin [48, 49], Kuznetsov [47, 50], or Sboui et al. [61] for various simplifications in the context of the lowest-order Raviart–Thomas method. Let $\widehat{\mathcal{T}}_H$ be a mesh consisting of general polygonal elements which can be nonconvex and

non star-shaped. We give an example in Figure 2 (dashed lines). The mesh $\widehat{\mathcal{T}}_H$ does not need to be matching, the maximal number of sides of each $K \in \widehat{\mathcal{T}}_H$ is not necessarily limited, and $\widehat{\mathcal{T}}_H$ is not necessarily shape-regular. We, however, assume that there exists a simplicial submesh $\mathcal{T}_h$ of $\widehat{\mathcal{T}}_H$ (that is, every element of $\widehat{\mathcal{T}}_H$ is triangulated by elements of $\mathcal{T}_h$) which is matching. An example is given in Figure 2 (solid lines). We recall in Section 5 that any order mixed finite elements can be written in the form

$$
\begin{pmatrix} \widehat{\mathbb{A}} & \widehat{\mathbb{B}}^t \\ \widehat{\mathbb{B}} & 0 \end{pmatrix} \begin{pmatrix} \widehat{U} \\ \widehat{P} \end{pmatrix} = \begin{pmatrix} \widehat{F} \\ \widehat{G} \end{pmatrix}, \tag{1.12}
$$

where $\widehat{U}$ is an algebraic vector of flux unknowns related to the *sides of* $\widehat{\mathcal{T}}_H$ only and $\widehat{P}$ is an algebraic vector of potential unknowns related to the *elements of* $\widehat{\mathcal{T}}_H$ only. The above system is of *indefinite, saddle point* type. In the lowest-order case and when the sides of $\mathcal{T}_h$ do not cut the sides of $\widehat{\mathcal{T}}_H$, there is one unknown in $\widehat{U}$ per side of $\widehat{\mathcal{T}}_H$ and one unknown in $\widehat{P}$ per element of $\widehat{\mathcal{T}}_H$. Similarly, we also recall in Section 5 that mixed finite elements can be written in the form

$$
\widehat{\mathbb{Z}}\widehat{\Lambda} = \widehat{E}, \tag{1.13}
$$

where $\widehat{\Lambda}$ is an algebraic vector of Lagrange multipliers related to the *sides of* $\widehat{\mathcal{T}}_H$ only. Here $\widehat{\mathbb{Z}}$ is *symmetric* and *positive definite*. Once again, in the lowest-order case and when the sides of $\mathcal{T}_h$ do not cut the sides of $\widehat{\mathcal{T}}_H$, there is one unknown in $\widehat{\Lambda}$ per side of $\widehat{\mathcal{T}}_H$. These properties are generally known in the mixed finite element community; they are typically used in domain decomposition algorithms (cf. [39]). Their proof, which we recall in Section 5, is immediate; it suffices to consider (1.3) or (1.6) on the mesh $\mathcal{T}_h$ and one obtains (1.12) or (1.13) by a simple *static condensation*. Moreover, it turns out that both (1.12) and (1.13) can, at least in certain situations, be reduced to

$$
\widehat{\mathbb{S}}\widehat{P} = \widehat{H}, \tag{1.14}
$$

i.e., to a system with one unknown per each polygon in $\widehat{\mathcal{T}}_H$ in the lowest-order case, by the techniques described in this paper.

The last goal of the present paper is to, through the preceding developments, show the *closeness of mixed finite element methods* to *various other discretization schemes*, namely mimetic finite difference [43, 20, 40], hybrid finite volume [35], mixed finite volume [31], multi-point flux-approximation [1, 2, 46, 3, 44, 5, 22, 15] and related methods [33, 51, 17, 68, 52], which in particular also enable the discretization on arbitrary polygonal meshes and are defined under one of the forms (1.12), (1.13), or (1.14). For arbitrary polygonal meshes, it seems that the only *conceptual difference* of the present mixed finite element approach with some of these methods is that in the mixed finite element method, one has to *construct a simplicial submesh* of each polygonal cell and to *solve a local problem* (invert a local matrix) on each polygonal cell. For some other comparisons between these various methods, we refer to [45, 32] and the references therein. Our main belief is that through these different links, the results and tools available in mixed finite element methods and those available in the context of the previously-cited methods can become mutually available: for mixed finite element methods, let us cite, e.g., the well-posedness of (1.3)/(1.5)/(1.6)/(1.10)/(1.11) on simplicial meshes, well-posedness of both (1.12) and (1.13) on arbitrary polygonal meshes, discrete maximum principle in the lowest-order case (see Section 3.3 below), optimal convergence and superconvergence a priori error estimates (see, e.g., [19, 58, 28, 29, 66]), optimal a posteriori error estimates [65, 7, 66], multigrid methods (see, e.g., [18, 26]), parallel implementations (see, e.g., [39]), multiscale and mortar versions (see, e.g., [11]), and convergence of adaptive methods [23, 16, 25]; for the previously-cited finite volume-type methods, let us cite in particular convergence analysis for nonlinear parabolic equations and their systems, see, e.g., [36, 37, 21].

Some conclusions of this paper are drawn in Section 7. An extension of the present ideas to higher-order cases and to more involved problems is the subject of the forthcoming work [69].

2 Notation

This section is devoted to collecting in one place the different notation used throughout the paper.

For a given domain $\omega \subset \mathbb{R}^d$, let $L^2(\omega)$ be the space of square-integrable (in the Lebesgue sense) functions over ω and $(\cdot, \cdot)_\omega$ the $L^2(\omega)$ inner product. We keep the same notations for $\mathbf{L}^2(\omega) := [L^2(\omega)]^d$ as well; we omit the index ω when $\omega = \Omega$. By $|\omega|$, we denote the Lebesgue measure of ω and by $|\sigma|$ the $(d-1)$-dimensional Lebesgue measure of a $(d-1)$-dimensional surface σ in $\mathbb{R}^d$. The symbol $|S|$ also stands for the cardinality (the number of elements) of a set S. Next, we let $\mathbf{H}(\mathrm{div}, \omega) := \{\mathbf{v} \in \mathbf{L}^2(\omega); \nabla \cdot \mathbf{v} \in L^2(\omega)\}$ be the space of functions with square-integrable weak divergences. We denote by $\langle \cdot, \cdot \rangle_\sigma$ the $(d-1)$-dimensional $L^2(\sigma)$-inner product on $\sigma \subset \mathbb{R}^{d-1}$.

Let $\mathcal{T}_h$ be a simplicial mesh of Ω, i.e., the elements of $\mathcal{T}_h$ are triangles in two space dimensions, tetrahedra in three space dimensions, and, in general, d-simplices. We suppose that $\mathcal{T}_h$ is matching, i.e., such that if $K, L \in \mathcal{T}_h$, $K \neq L$, then $K \cap L$ is either an empty set or a common vertex of K and L or a common d'-face of the mesh $\mathcal{T}_h$, $1 \leq d' \leq d-1$. We denote by $\mathcal{E}_h$ the set of all sides of $\mathcal{T}_h$, i.e., the set of $(d-1)$-faces of the mesh $\mathcal{T}_h$. We divide $\mathcal{E}_h$ into interior sides $\mathcal{E}_h^{\mathrm{int}}$ and boundary sides $\mathcal{E}_h^{\mathrm{ext}}$. Let $\sigma \in \mathcal{E}_h$ and let ψ be a possibly double-valued function on σ. We denote by $[\![\psi]\!]$ the jump of the function ψ over the side σ, i.e., the difference of the values of ψ on both sides of σ (the arbitrariness of the sign is irrelevant in what follows) when $\sigma \in \mathcal{E}_h^{\mathrm{int}}$, and the value that ψ takes on σ when $\sigma \in \mathcal{E}_h^{\mathrm{ext}}$. Let $K \in \mathcal{T}_h$. By $\mathcal{E}_K$, we denote the set of all sides of K and by $\mathcal{E}_K^{\mathrm{int}}$ the set of such sides of $\mathcal{E}_K$ which lie in $\mathcal{E}_h^{\mathrm{int}}$. For $K \in \mathcal{T}_h$, let $\mathbf{n}_K$ be the unit normal vector defined on the sides of K, outward to K, and, for $\sigma \in \mathcal{E}_h$, let $\mathbf{n}_\sigma$ stand for the unit normal vector of σ whose orientation is chosen arbitrarily but fixed for interior sides and coinciding with the exterior normal of Ω for boundary sides. We next denote by $\mathcal{V}_h$ the set of vertices of $\mathcal{T}_h$. For a given vertex $V \in \mathcal{V}_h$, we shall denote by $\mathcal{T}_V$ the patch of the elements of $\mathcal{T}_h$ which share V, by $\mathcal{E}_V$ those sides of the elements in $\mathcal{T}_V$ contained in $\mathcal{E}_h^{\mathrm{int}}$, by $\mathcal{E}_V^{\mathrm{int}}$ the sides in the interior of $\mathcal{T}_V$, and by $\mathcal{E}_V^{\mathrm{ext}}$ the set $\mathcal{E}_V \setminus \mathcal{E}_V^{\mathrm{int}}$. We will also employ the notation $\mathcal{E}_{V,K}$ for the sides of K which have V as vertex. For $K \in \mathcal{T}_h$, we denote by $\mathbf{x}_K$ the barycenter of K and for $\sigma \in \mathcal{E}_h$, we denote by $\mathbf{x}_\sigma$ the barycenter of σ. By $\mathbb{P}_k(\mathcal{T}_h)$, we denote the space of piecewise polynomials on $\mathcal{T}_h$ of degree k and by $\mathbb{P}_k(\mathcal{E}_h^{\mathrm{int}})$ the space of piecewise polynomials on $\mathcal{E}_h^{\mathrm{int}}$ of degree k. We will use the notation $\mathbb{I}$ for the identity matrix.

3 Reminders on the lowest-order mixed finite element method

We give in this section some reminders on the lowest-order Raviart–Thomas mixed finite element method. We first give its definition. Then, in Section 3.1, we recall its relation to the Crouzeix–Raviart nonconforming finite element method, in Section 3.2, we present the local flux expressions from the Lagrange multipliers, and, in Section 3.3, we recall the different variants of the discrete maximum principle valid herein.

In the lowest-order Raviart–Thomas mixed finite element method (see [57] for $d = 2$ and [55] for $d = 3$), we have $\Phi_h = \mathbb{P}_0(\mathcal{T}_h)$, $\Psi_h = \mathbb{P}_0(\mathcal{E}_h^{\mathrm{int}})$, and, for $K \in \mathcal{T}_h$, $\mathbf{V}_h(K) = \mathbb{P}_0^d + \mathbb{P}_0\mathbf{x}$. Concerning the space $\mathbf{V}_h$, there is one basis function $\mathbf{v}_\sigma$ associated with each $\sigma \in \mathcal{E}_h$. For $\sigma_{K,L} \in \mathcal{E}_h^{\mathrm{int}}$, $\mathbf{v}_{\sigma_{K,L}}(\mathbf{x}) = \frac{1}{d|K|}(\mathbf{x} - V_K)$, $\mathbf{x} \in K$, $\mathbf{v}_{\sigma_{K,L}}(\mathbf{x}) = \frac{1}{d|L|}(V_L - \mathbf{x})$, $\mathbf{x} \in L$, $\mathbf{v}_{\sigma_{K,L}}(\mathbf{x}) = 0$ otherwise, where V_K is the vertex of K opposite to $\sigma_{K,L}$ and V_L the vertex of L opposite to $\sigma_{K,L}$. The orientation of $\mathbf{v}_{\sigma_{K,L}}$ (the order of K and L) is arbitrary but fixed. For a boundary side σ, the support of $\mathbf{v}_\sigma$

only consists of $K \in \mathcal{T}_h$ such that $\sigma \in \mathcal{E}_K$. We refer to [19, 58] for more details.

3.1 Relation to the Crouzeix–Raviart nonconforming finite element method

Let $\tilde{\Psi}_h$ be the Crouzeix–Raviart nonconforming space (see [30]), i.e., the space of piecewise affine functions on $\mathcal{T}_h$ such that all $\tilde{\psi}_h \in \tilde{\Psi}_h$ verify

$$\langle [\![\tilde{\psi}_h]\!], 1 \rangle_\sigma = 0 \qquad \forall \sigma \in \mathcal{E}_h.$$

There is one basis function associated with each $\sigma \in \mathcal{E}_h^{\text{int}}$, denoted by $\tilde{\psi}_\sigma$. It is such that $\tilde{\psi}_\sigma(\mathbf{x}_\sigma) = 1$ and $\tilde{\psi}_\sigma(\mathbf{x}_\gamma) = 0$ for all sides $\gamma \in \mathcal{E}_h$ different from σ (recall that $\mathbf{x}_\sigma$ stands for the barycenter of the side σ).

The Crouzeix–Raviart nonconforming finite element method (see [30, 27]) for the problem (1.1a)–(1.1b) reads: find $\tilde{\lambda}_h \in \tilde{\Psi}_h$ such that

$$(\mathbf{S}\nabla\tilde{\lambda}_h, \nabla\tilde{\psi}_h) = (g, \tilde{\psi}_h) \qquad \forall \tilde{\psi}_h \in \tilde{\Psi}_h. \tag{3.1}$$

In a matrix setting, it can be written as

$$\mathbb{Z}\Lambda = E. \tag{3.2}$$

It follows from [13, 9, 26, 38, 67] that the above matrix $\mathbb{Z}$ and the right-hand side vector E completely coincide with the $\mathbb{Z}$ and E of (1.6). Consequently, the same holds true for the solution Λ of (1.6) and that of (3.2). This means that, in the present setting (both $\mathbf{S}$ and g are piecewise constant on $\mathcal{T}_h$), the Crouzeix–Raviart nonconforming finite element method (3.2) is *completely equivalent* with the hybridization (1.6) of the lowest-order Raviart–Thomas mixed finite element one. Let $\sigma \in \mathcal{E}_h^{\text{int}}$ and denote the value of λ_h in the barycenter of σ by λ_σ. In order to simplify notation later on, in link with the homogeneous Dirichlet boundary condition (1.1b), let us set $\lambda_\sigma = 0$ for all $\sigma \in \mathcal{E}_h^{\text{ext}}$. With this notation, we can obtain $\tilde{\lambda}_h$ from the Lagrange multipliers λ_h given by (1.5) or by (1.6) by

$$\tilde{\lambda}_h = \sum_{\sigma \in \mathcal{E}_h^{\text{int}}} \lambda_\sigma \tilde{\psi}_\sigma. \tag{3.3}$$

We note that for more general coefficients or equations, there is still no structural difference. There may be a small difference in the coefficients of the involved matrices and right-hand sides which can be analyzed within the abstract framework of variational crimes. We refer for more details to [9].

3.2 Local flux expressions from the Lagrange multipliers

The developments of the previous section allow to readily infer (cf., e.g., [13, 54, 26]) that the flux $\mathbf{u}_h$ and the potential p_h in the lowest-order Raviart–Thomas mixed finite element method can be locally expressed from $\tilde{\lambda}_h$. Denote, for $K \in \mathcal{T}_h$, $q_K(\mathbf{x}) := (\mathbf{x} - \mathbf{x}_K)^t \mathbf{S}_K^{-1}(\mathbf{x} - \mathbf{x}_K)$, where $\mathbf{S}_K := \mathbf{S}|_K$. Then

$$\mathbf{u}_h|_K = -\mathbf{S}_K \nabla\tilde{\lambda}_h|_K + \frac{g_K}{d}(\mathbf{x} - \mathbf{x}_K), \tag{3.4a}$$

$$p_h|_K = \tilde{\lambda}_h(\mathbf{x}_K) + \frac{g_K}{2d|K|}(q_K, 1)_K, \tag{3.4b}$$

where $g_K := g|_K$ (recall that $\mathbf{x}_K$ is the barycenter of the element K, d the space dimension, and $|K|$ the measure of the element K). Relation (3.4a) in particular means that there exist *local*

flux expressions from the *Lagrange multipliers.* Relation (3.4b) means that the original potential approximation p_h *is linked* to the *Lagrange multipliers* and, additionally, to the *source term.* By combining (3.4a) and (3.4b), we see how $\mathbf{u}_h$ is locally linked to p_h. It is, however, not obvious how to express locally $\mathbf{u}_h$ from p_h.

3.3 The discrete maximum principle

Let $\mathbf{S}$ be such that it can be written as $\mathbb{I}$ (the identity matrix) times a piecewise constant scalar function and let $\mathcal{T}_h$ be acute, i.e., such that the magnitude of the angles between $\mathbf{n}_{K,\sigma}$, $\sigma \in \mathcal{E}_K$, for all $K \in \mathcal{T}_h$ is greater or equal to $\pi/2$ (all interior angles smaller or equal to $\pi/2$ in two space dimensions). As another consequence of the above equivalence, we immediately have that the *discrete maximum principle* holds for the *Lagrange multipliers* λ_h, i.e., for the values λ_σ, $\sigma \in \mathcal{E}_h$. This is a classical result, shown in a more general setting in, e.g., [38, Theorem 4.5]. Note that one does not necessarily have the discrete maximum principle for the function $\tilde{\lambda}_h$ defined in (3.3), as this function may take values larger than $\max_{\sigma \in \mathcal{E}_h} \lambda_\sigma$ and smaller than $\min_{\sigma \in \mathcal{E}_h} \lambda_\sigma$ (see Figure 1, right for a graphical illustration) (only the punctual values of $\tilde{\lambda}_h$ in side barycenters satisfy the discrete maximum principle).

Consider now for simplicity $\mathbf{S} = \mathbb{I}$, the source term g constant in the whole Ω, $d = 2$, and the case where $\mathcal{T}_h$ is Delaunay (that is, the circumcircle of each triangle does not contain any vertex in its interior) and the additional condition that no circumcenters of boundary triangles lie outside the domain. Then, following [72] (we give more details below), the lowest-order Raviart–Thomas mixed finite element method is also equivalent to the classical two-point finite volume scheme (see [34]). Thus, one also has the *discrete maximum principle* for the *values of $\tilde{\lambda}_h$ in the circumcenters* of the elements of $\mathcal{T}_h$.

Finally, note that by properties of a simplex and by the fact that $\tilde{\lambda}_h$ is an affine function,

$$\tilde{\lambda}_h(\mathbf{x}_K) = \frac{1}{d+1} \sum_{\sigma \in \mathcal{E}_K} \lambda_\sigma$$

for all $K \in \mathcal{T}_h$. Recall that the formula (3.4b) relates $\tilde{\lambda}_h$ and p_h. Thus, it follows that for acute meshes and multiples of the identity matrix diffusion tensors, the *discrete maximum principle* also holds for the *original approximation p_h* whenever the *source term g is zero.* However, because of the presence of g in (3.4b), there is in general *no discrete maximum principle* for the *original approximation p_h* in the presence of a *nonzero source term.* Note, however, that if $g \geq 0$, then one still has $p_h \geq 0$ by (3.4b) and by the above discrete maximum principle for $\tilde{\lambda}_h(\mathbf{x}_K)$.

4 Reductions of the lowest-order mixed finite element method

We present here a unified framework allowing to reduce (1.3), (1.5), or (1.6) in the lowest-order Raviart–Thomas mixed finite element method equivalently to (1.10) or (1.11).

Firstly, in Section 4.1, we define *local problems* on *patches of elements* (in practice, local matrices need to to be assembled and inverted) which give *local flux expressions.* In this feature, our approach is similar to that of the multi-point flux-approximation method [1, 2, 46, 3, 44, 5, 22, 15] or to [33, 51, 17, 68, 52], and we investigate this link in Section 4.1. Next, in Section 4.1.1, we show that the approach of [72, 24, 71] falls into our framework and leads to local matrices which are diagonal. Also the approach of [64] is included in the present framework, see Section 4.1.2, and leads to local matrices which are not diagonal. Taking these approaches one step further, following [70], we show in Section 4.1.3 that the properties of the local matrices (and consequently
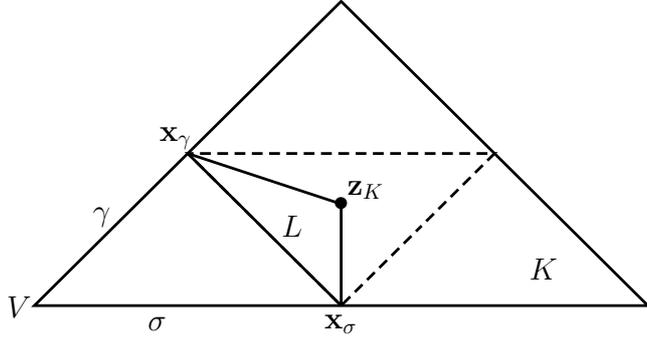
Figure 3: Triangle $K \in \mathcal{T}_h$ and subtriangle L given by two edge midpoints $\mathbf{x}_\sigma$ and $\mathbf{x}_\gamma$ and the point $\mathbf{z}_K$

the properties of the final matrices $\bar{\mathbb{S}}$ or $\mathbb{S}$) can be influenced so as to be as good as possible with respect to the local geometry of the mesh $\mathcal{T}_h$ and to the local behavior of the diffusion tensor $\mathbf{S}$. This also represents a conceptual step in order to avoid the possible appearance of singular local and global matrices [72, 24, 71, 64]. Previous examples of locally influencing the final system properties include, e.g., [35, 4, 32]. Further, following [70], we generalize this approach in Section 4.2, staying on a purely algebraic level.

Section 4.3 shows how to express the Lagrange multipliers Λ or the fluxes U from the (new) potential unknowns $\bar{P}$ in the whole mesh, while only using the above local problems, which improves on (1.7). We use these expressions in Section 4.4 and present two conceptually different ways of obtaining the final *one-unknown-per-element* systems (1.10) or (1.11). Finally, we discuss the symmetry and positive definiteness of the final matrices in Section 4.5.

4.1 Local problems definition by a geometrical interpretation and the link to the multi-point flux-approximation method

Consider the lowest-order Raviart–Thomas mixed finite element method for the problem (1.1a)–(1.1b), i.e., (1.2a)–(1.2b) with the spaces Φ_h, $\mathbf{V}_h$ specified in Section 3 and leading to a linear system of a form (1.3), (1.5), or (1.6).

Let $K \in \mathcal{T}_h$ be fixed. Recalling the definition (3.3) of $\tilde{\lambda}_h$ and taking into account that $\tilde{\lambda}_h|_K$ is an affine function, it can be fixed by its nodal values in $d+1$ points which do not lie in the same hyperplane of $\mathbb{R}^d$ (line in two space dimensions). In (3.3), these $d+1$ values are the $d+1$ Lagrange multipliers λ_σ, $\sigma \in \mathcal{E}_K$, i.e., we fix $\tilde{\lambda}_h|_K$ by its point values in the side barycenters (recall that we have set $\lambda_\sigma = 0$ for $\sigma \in \mathcal{E}_h^{\text{ext}}$). Let $\mathbf{z}_K$ be a point arbitrary in $\mathbb{R}^d$ but such that any d of the $d+1$ side barycenters of K, denoted by $\mathbf{x}_\sigma$, and the point $\mathbf{z}_K$ do not lie in the same hyperplane. In two space dimensions, this means that any two of the three edge midpoints $\mathbf{x}_\sigma$ and $\mathbf{z}_K$ do not lie in the same line, i.e., that $\mathbf{z}_K$ does not lie on the boundary of the dashed triangle in Figure 3. Suppose now a *new unknown value* $\bar{p}_K$ in any $K \in \mathcal{T}_h$. Let V be any of the vertices of K and denote by $\mathcal{E}_{V,K}$ the sides of K which have V as vertex. Then $\tilde{\lambda}_h|_K$ can also be uniquely prescribed by the value $\bar{p}_K$ it takes in the point $\mathbf{z}_K$ and by the values of the d Lagrange multipliers λ_σ associated with the side barycenters $\mathbf{x}_\sigma$ of $\sigma \in \mathcal{E}_{V,K}$. In the notation of Figure 3, we are saying that $\tilde{\lambda}_h|_K$ can be uniquely prescribed by the values it takes in the points $\mathbf{z}_K$, $\mathbf{x}_\sigma$, and $\mathbf{x}_\gamma$. In terms of $\tilde{\lambda}_h$, the new unknown is thus

$$\bar{p}_K := \tilde{\lambda}_h(\mathbf{z}_K). \tag{4.1}$$

Let a new simplex L (subsimplex of K) be given by the side barycenters $\mathbf{x}_\sigma$, $\sigma \in \mathcal{E}_{V,K}$, and
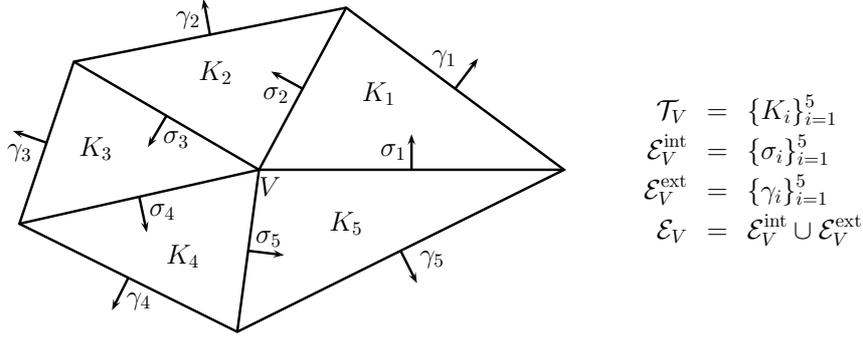
9

Figure 4: An example of a patch $\mathcal{T}_V$ around a vertex V

by the point $\mathbf{z}_K$, see Figure 3 (here the points are denoted by $\mathbf{z}_K$, $\mathbf{x}_\sigma$, and $\mathbf{x}_\gamma$). Denote by $\tilde{\varphi}_\sigma$, $\sigma \in \mathcal{E}_{V,K}$, and by $\tilde{\varphi}_K$ the Lagrange basis functions associated with the points $\mathbf{x}_\sigma$, $\sigma \in \mathcal{E}_{V,K}$, and $\mathbf{z}_K$; we consider $\tilde{\varphi}_\sigma$ and $\tilde{\varphi}_K$ supported on K (and not on L). More precisely, $\tilde{\varphi}_\sigma$, $\sigma \in \mathcal{E}_{V,K}$, is the affine function which takes value 1 in $\mathbf{x}_\sigma$, value 0 in $\mathbf{x}_\gamma$, $\gamma \in \mathcal{E}_{V,K}$, $\gamma \neq \sigma$, and value 0 in $\mathbf{z}_K$. Similarly, $\tilde{\varphi}_K$ takes value 1 in $\mathbf{z}_K$ and value 0 in $\mathbf{x}_\sigma$, $\sigma \in \mathcal{E}_{V,K}$. Then, using (3.4a), we get

$$\mathbf{u}_h|_K = -\mathbf{S}_K \nabla \left(\sum_{\sigma \in \mathcal{E}_{V,K}} \lambda_\sigma \tilde{\varphi}_\sigma + \bar{p}_K \tilde{\varphi}_K \right) + \frac{g_K}{d}(\mathbf{x} - \mathbf{x}_K). \tag{4.2}$$

Let now a vertex $V \in \mathcal{V}_h$ be fixed and consider the patch $\mathcal{T}_V$; we recall that these are the elements of $\mathcal{T}_h$ which share V. We refer to Figure 4 for an example. Suppose we have chosen a point $\mathbf{z}_K$ for each $K \in \mathcal{T}_V$, as described above. Suppose that $\tilde{\lambda}_h$ is expressed using the values in $\mathbf{z}_K$, $K \in \mathcal{T}_V$, and in those side barycenters $\mathbf{x}_\sigma$ which lie in the internal sides of the patch $\mathcal{T}_V$ or in the sides lying in $\partial\Omega$. For Figure 4, these are the sides σ_i, $i = 1, \ldots, 5$. Recall that we then have (4.2) for any $K \in \mathcal{T}_V$. Consider the equations (1.4c) associated with ψ_h associated with the internal sides of the patch $\mathcal{T}_V$ (recall that we have denoted these sides by $\mathcal{E}_V^{\text{int}}$). This gives rise to the following *local problem*: given $\bar{p}_K$, $K \in \mathcal{T}_V$, find λ_γ, $\gamma \in \mathcal{E}_V^{\text{int}}$, such that

$$\sum_{K \in \mathcal{T}_V; \, \sigma \in \mathcal{E}_K} \langle \mathbf{u}_h \cdot \mathbf{n}_K, 1 \rangle_\sigma = 0 \qquad \forall \sigma \in \mathcal{E}_V^{\text{int}}. \tag{4.3}$$

In the above summation, we, for a given $\sigma \in \mathcal{E}_V^{\text{int}}$, go through all elements $K \in \mathcal{T}_V$ such that σ is a side of K (there are two such elements K). Note that (4.3) (while plugging (4.2) therein) leads to a square linear system. Suppose that this linear system is well-posed. Then we can express the Lagrange multipliers λ_γ *inside the patch* $\mathcal{T}_V$ as a function of the new element values $\bar{p}_K$ *in the patch* $\mathcal{T}_V$ (and of the sources g_K in the patch $\mathcal{T}_V$). Considering (4.2), we can also get the fluxes $\mathbf{u}_h$ in the whole patch $\mathcal{T}_V$ as a function of $\bar{p}_K$, i.e., we obtain *local flux expressions* from the new element potentials $\bar{p}_K$.

Remark 4.1 (Relation to the multi-point flux-approximation method)**.** *Considering a patch of (sub)elements, supposing a piecewise affine, possibly nonconforming, potential approximation, imposing the normal flux continuity, and solving a local linear system on the patch is also the* principle *of the so-called multi-point flux-approximation method [1, 2] (or of the methods of [33, 51, 17]). This is for us a confirmation of the fact that lowest-order Raviart–Thomas* mixed finite elements *and multi-point flux-approximation* finite volume methods *are* conceptually *very* close. *We refer to Remarks 4.2 and 4.3 below for further precisions.*

Remark 4.2 (Strong potential–flux relation × variationally consistent potential–flux relation). *In the multi-point flux-approximation finite volume methods [1, 2, 33, 51, 17], the fluxes on patches of (sub)elements are locally recovered from the potentials in terms of a strong equality, only following the continuous potential–flux relation* $\mathbf{u} = -\mathbf{S}\nabla p$. *The essential difference of our approach is that we recover the fluxes from the potentials by a weak, variationally consistent formulation, following on the continuous level both the potential–flux relation* $\mathbf{u} = -\mathbf{S}\nabla p$ *and the divergence constraint* $\nabla \cdot \mathbf{u} = g$; *see also [64, Remark 2.3].*

Let us now elaborate on (4.2)–(4.3). First recall that (4.3) can be equivalently rewritten as

$$\sum_{K\in\mathcal{T}_V;\,\sigma\in\mathcal{E}_K} \langle \mathbf{u}_h \cdot \mathbf{n}_K, \tilde{\psi}_\sigma \rangle_{\partial K} = 0 \qquad \forall \sigma \in \mathcal{E}_V^{\text{int}}.$$

Here $\tilde{\psi}_\sigma$ are the Crouzeix–Raviart nonconforming basis functions, see Section 3.1. This follows by the fact that $\mathbf{u}_h \cdot \mathbf{n}_K$ is constant on any $\sigma \in \mathcal{E}_K$, by the fact that $\langle 1, \tilde{\psi}_\sigma \rangle_\sigma = |\sigma|$, and by the fact that $\langle 1, \tilde{\psi}_\sigma \rangle_\gamma = 0$ for any side γ different from σ, so that $\langle \mathbf{u}_h \cdot \mathbf{n}_K, 1 \rangle_\sigma = \langle \mathbf{u}_h \cdot \mathbf{n}_K, \tilde{\psi}_\sigma \rangle_\sigma = \langle \mathbf{u}_h \cdot \mathbf{n}_K, \tilde{\psi}_\sigma \rangle_{\partial K}$. Form this equality, using the Green theorem, we have

$$\sum_{K\in\mathcal{T}_V;\,\sigma\in\mathcal{E}_K} \{ (\nabla \cdot \mathbf{u}_h, \tilde{\psi}_\sigma)_K + (\mathbf{u}_h, \nabla\tilde{\psi}_\sigma)_K \} = 0 \qquad \forall \sigma \in \mathcal{E}_V^{\text{int}}. \tag{4.4}$$

It follows from (1.2b) and the definition of $\mathbf{V}_h(K)$ in Section 3 that $(\nabla \cdot \mathbf{u}_h)|_K = g_K$. For the other term in the above relation, we employ (4.2). Remark that

$$(\mathbf{x} - \mathbf{x}_K, \nabla\tilde{\psi}_\sigma)_K = 0,$$

as $(\nabla\tilde{\psi}_\sigma)|_K$ is a constant vector and $\mathbf{x}_K$ is the barycenter of K. Extend the notation $\tilde{\varphi}_\sigma$ from (4.2) to a Lagrange basis function supported on all $K \in \mathcal{T}_V$ such that $\sigma \in \mathcal{E}_K$. Remark that the functions $\tilde{\varphi}_\sigma$ are nonconforming. They are only continuous in the barycenters of the sides sharing the vertex V. They have the same support as $\tilde{\psi}_\sigma$, but are different from $\tilde{\psi}_\sigma$. We then see that (4.2)–(4.3) is equivalent to the following problem: given $\bar{p}_K$, $K \in \mathcal{T}_V$, find λ_γ, $\gamma \in \mathcal{E}_V^{\text{int}}$, such that

$$\sum_{K\in\mathcal{T}_V;\,\sigma\in\mathcal{E}_K} \sum_{\gamma\in\mathcal{E}_V^{\text{int}}} \lambda_\gamma (\mathbf{S}_K \nabla\tilde{\varphi}_\gamma, \nabla\tilde{\psi}_\sigma)_K = \sum_{K\in\mathcal{T}_V;\,\sigma\in\mathcal{E}_K} \{ (g_K, \tilde{\psi}_\sigma)_K - \bar{p}_K (\mathbf{S}_K \nabla\tilde{\varphi}_K, \nabla\tilde{\psi}_\sigma)_K \} \qquad \forall \sigma \in \mathcal{E}_V^{\text{int}}. \tag{4.5}$$

Remark that (4.5) is a *Petrov–Galerkin problem*, as the basis functions $\tilde{\psi}_\sigma$ of the test space are different from the basis functions $\tilde{\varphi}_\gamma$ of the trial space. We can now also infer the matrix form of (4.5): given $\bar{P}_V = \{\bar{p}_K\}_{K\in\mathcal{T}_V}$, find $\Lambda_V^{\text{int}} = \{\lambda_\gamma\}_{\gamma\in\mathcal{E}_V^{\text{int}}}$ such that

$$\mathbb{M}_V \Lambda_V^{\text{int}} = \widetilde{G}_V - \mathbb{J}_V \bar{P}_V, \tag{4.6}$$

where

$$(\mathbb{M}_V)_{\sigma,\gamma} := \sum_{K\in\mathcal{T}_V;\,\sigma\in\mathcal{E}_K} (\mathbf{S}_K \nabla\tilde{\varphi}_\gamma, \nabla\tilde{\psi}_\sigma)_K, \tag{4.7a}$$

$$(\widetilde{G}_V)_\sigma := \sum_{K\in\mathcal{T}_V;\,\sigma\in\mathcal{E}_K} (g_K, \tilde{\psi}_\sigma)_K, \tag{4.7b}$$

$$(\mathbb{J}_V)_{\sigma,K} := -(\mathbf{S}_K \nabla\tilde{\varphi}_K, \nabla\tilde{\psi}_\sigma)_K. \tag{4.7c}$$

In Figure 5, we illustrate for later use the gradients of the basis functions $\tilde{\psi}_\sigma$ and $\tilde{\varphi}_\sigma$.
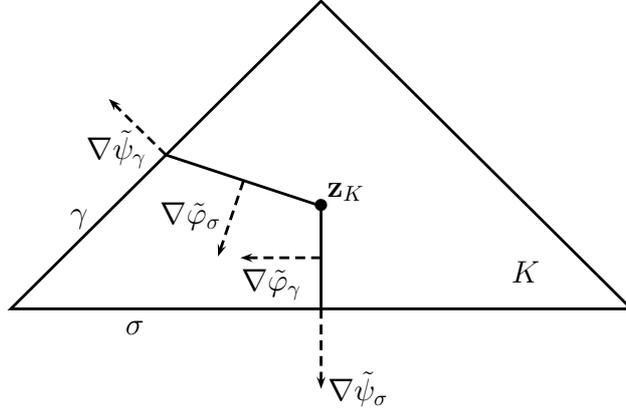
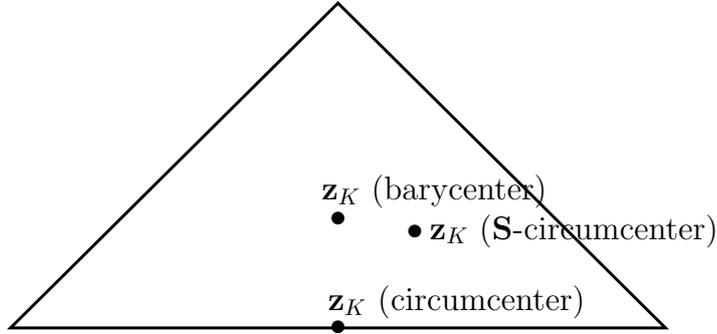Figure 5: Basis functions gradients in an element $K \in \mathcal{T}_h$

Figure 6: Circumcenter, $\mathbf{S}$-circumcenter, and barycenter as the evaluation points $\mathbf{z}_K$

In the above developments, we have not specified the choice of the points $\mathbf{z}_K$. It turns out that, in a formulation different from (4.2)–(4.3) (or, equivalently, (4.5)), three particular choices of $\mathbf{z}_K$ (the circumcenter, the so-called $\mathbf{S}$-circumcenter, and the barycenter) have already been studied previously in the literature in [72, 24, 71] and [64], respectively. We plot these three choices in Figure 6 for the example of the triangle of Figure 3 and for the diffusion tensor $\mathbf{S}$ given by

$$\mathbf{S} = \left(\begin{array}{cc} 0.7236 & 0.3804 \\ 0.3804 & 0.4764 \end{array} \right),$$

which corresponds to the first form $\mathbf{S}$ takes in (6.2) below. We now present these and other choices in more details. In parallel with the present work, we give a detailed study of the properties of the corresponding local condensation matrices $\mathbb{M}_V$ in [70]. For the moment, we only remark that $\mathbb{M}_V$ can be all *diagonal*, *nonsymmetric*, *regular*, or *singular*.

4.1.1 S-circumcenter as the evaluation point

It turns out that in [72, 24] for two space dimensions and in [71] for three space dimensions, the problem (4.2)–(4.3) (or, equivalently (4.5)) was studied in a different form. The first one to observe that the approach of [72, 24, 71] falls into the framework (4.2)–(4.3) was probably [53]. In [72, 24, 71], a starting additional condition or assumption was that the matrix $\mathbb{M}_V$ given by (4.7a) is *diagonal*.

It turns out that in two space dimensions, one can always find a point $\mathbf{z}_K$ such that $\mathbb{M}_V$ is diagonal, or, equivalently, such that the basis functions in the Petrov–Galerkin problem (4.5) are
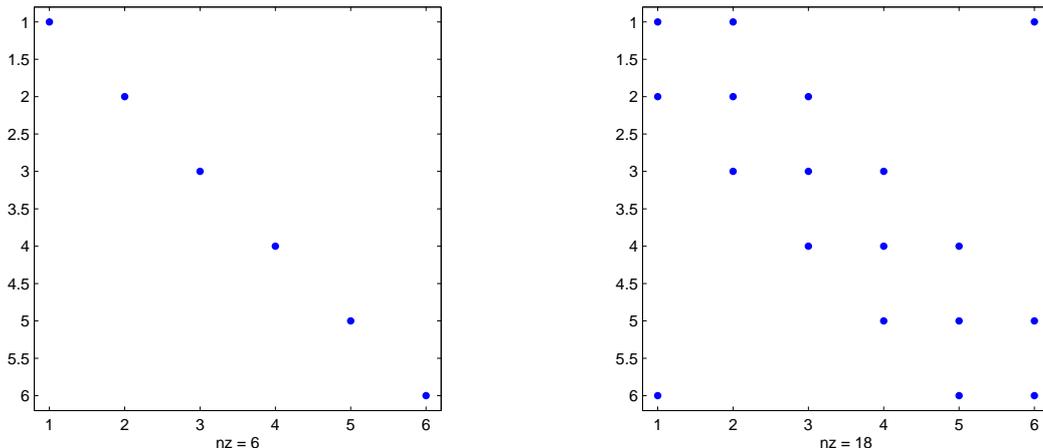
Figure 7: Typical local condensation matrices sparsity patterns, **S**-circumcenter (left) and barycenter (right) as the evaluation points $\mathbf{z}_K$

orthogonal with respect to the $(\mathbf{S}\cdot,\cdot)$ scalar product. When $\mathbf{S}_K = \mathbb{I}s_K$, $\mathbf{z}_K$ is the *circumcenter* of K. This can be easily seen from Figure 5: when $\mathbf{z}_K$ is the circumcenter of K, $\nabla\tilde{\psi}_\sigma$ is orthogonal to $\nabla\tilde{\varphi}_\gamma$ and $\nabla\tilde{\psi}_\gamma$ is orthogonal to $\nabla\tilde{\varphi}_\sigma$, i.e., $\nabla\tilde{\varphi}_\gamma \cdot \nabla\tilde{\psi}_\sigma = 0$ and $\nabla\tilde{\varphi}_\sigma \cdot \nabla\tilde{\psi}_\gamma = 0$; consequently, the off-diagonal terms of $\mathbb{M}_V$ vanish. A point $\mathbf{z}_K$ such that $\mathbb{M}_V$ is diagonal can still be found for a general full-matrix $\mathbf{S}_K$. It is determined by the requirements $\mathbf{S}_K\nabla\tilde{\varphi}_\gamma \cdot \nabla\tilde{\psi}_\sigma = 0$ and $\mathbf{S}_K\nabla\tilde{\varphi}_\sigma \cdot \nabla\tilde{\psi}_\gamma = 0$, with the notation of Figure 5. We call this point **S**-*circumcenter*; the whole mesh $\mathcal{T}_h$ then becomes "**S**-orthogonal grid" in the terminology of [1]. The **S**-circumcenter is uniquely defined in each triangle by the above requirement.

In the approach of this section *no local linear system needs to be solved* and one always obtains a *two-point flux expression*, i.e., the flux over a given side $\sigma_{K,L} \in \mathcal{E}_h^{\text{int}}$ is only expressed using the potentials $\bar{p}_K$ and $\bar{p}_L$ associated with the two simplices K and L sharing $\sigma_{K,L}$. Thus, in two space dimensions, lowest-order Raviart–Thomas mixed finite elements give two-point flux expressions even on unstructured triangular meshes with a full-matrix diffusion tensor **S**. Remark finally that in this case, the *choice of the evaluation point* $\mathbf{z}_K$ *depends on the diffusion tensor* **S** (but not on the local geometry). The sparsity pattern of a typical local condensation matrix $\mathbb{M}_V$ in this case is given in Figure 7, left.

For the analysis of the well-posedness of (4.6) and of the properties of $\mathbb{M}_V$ with this choice of $\mathbf{z}_K$, we refer to [72, 24, 71] and to [70]. Unfortunately, it turns out that proceeding with a diagonal matrix $\mathbb{M}_V$ is *not possible* in *three* (and higher) *space dimensions* unless a specific geometric situation occurs. Examples are given in [71]. This geometric situation can be identified, for $\mathbf{S}_K = \mathbb{I}s_K$, as the requirement that the circumcenter of each side of K coincides with the barycenter of this side. Moreover, even in two space dimensions, this approach can *degenerate*. This happens when $\mathbf{z}_K$ coincides with one of the side barycenters $\mathbf{x}_\sigma$, as illustrated in Figure 6. Then, with the notation of Figure 3, the measure of the subtriangle L becomes 0, $|L| = 0$. Consequently, one obtains $|\nabla\tilde{\varphi}_\sigma| = \infty$. Figure 8 represents a typical mesh / situation where this happens. A remedy by "aggregation" of the two triangles into a square is suggested in [24], see Figure 8.

4.1.2 Barycenter as the evaluation point

The choice of $\mathbf{z}_K = \mathbf{x}_K$, i.e., $\mathbf{z}_K$ as the barycenter, is related to the approach studied in [64].
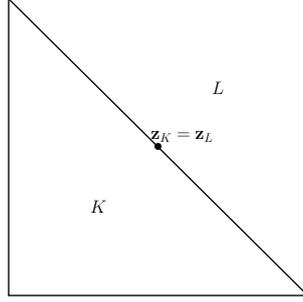
Figure 8: Two triangles cutting a square and the coinciding circumcenters

It turns out that the choice $\mathbf{z}_K$ as the barycenter allows for a wider variety of meshes for which the local problems (4.6) are well-posed and that it works in three (d in general) space dimensions, without any difference to two space dimensions. The matrix $\mathbb{M}_V$ is *not diagonal* in general (it gets diagonal when $\mathbf{S}_K = \mathbb{I}s_K$ and when the barycenters coincide with the circumcenters, i.e., on equilateral simplices). This leads to the necessity to *solve local linear systems* and to a *multi-point flux expression*, i.e., to the situation where the fluxes can only be expressed from the potentials $\bar{p}_K$ of the whole patch $\mathcal{T}_V$. The *choice of the evaluation point* $\mathbf{z}_K$ *depends neither on the diffusion tensor* $\mathbf{S}$, *nor on the local geometry*. This approach can, however, lead to a *singular local condensation matrix* $\mathbb{M}_V$. This happens, e.g., for $\mathbf{S} = \mathbb{I}$ and the patch $\mathcal{T}_V$ illustrated in Figure 9. The sparsity pattern of a typical local condensation matrix $\mathbb{M}_V$ in this case is given in Figure 7, right.

For the analysis of the well-posedness of (4.6) and of the properties of $\mathbb{M}_V$ with this choice of $\mathbf{z}_K$, we refer to [64] and to [70]. In [64], one expresses $\mathbf{u}_h|_{\mathcal{T}_V}$ directly from the *original unknowns* $p_K := p_h|_K$, $K \in \mathcal{T}_V$. Noting that for the barycenter ($\mathbf{z}_K = \mathbf{x}_K$) and when $g = 0$, we have from (3.4b) $p_K = \bar{p}_K = \tilde{\lambda}_h(\mathbf{z}_K)$, it can be shown that the local problems (4.2)–(4.3) (or, equivalently (4.5)) coincide with those given in [64] (see namely Remark 3.5 in this reference), although the presentation in [64] is different from that given here. When $g \neq 0$, it follows from (3.4b) that p_K and $\bar{p}_K = \tilde{\lambda}_h(\mathbf{z}_K)$ only differ by the known constants given by $g_K(q_K, 1)_K/2d|K|$. Consequently, the local problems (4.2)–(4.3) and those of [64] can still be written in the form (4.6) with the same local matrices $\mathbb{M}_V$ given by (4.7a) and only differ by the vectors $\bar{P}_V$ and the right-hand side.

Remark 4.3 (Singular matrices in the multi-point flux-approximation method)**.** *Consider a triangular mesh and the case where* $g = 0$. *It was shown in [42], based on the results of [64], that the nonsymmetric multi-point flux-approximation O-method [1, 2] is completely equivalent to the lowest-order Raviart–Thomas mixed finite elements written with one unknown per element, with* $\mathbf{z}_K$ *being the barycenters. Thus, this variant of the* multi-point flux-approximation method *also gives rise to a* singular matrix $\mathbb{M}_V$ *(and singular final matrix, see Section 4.4.1 below) for the mesh of Figure 9.*

4.1.3 Changing the evaluation point according to the local geometry and diffusion tensor

In the framework of the Crouzeix–Raviart nonconforming finite element method (equivalent to the lowest-order Raviart–Thomas method, see Section 3.1), a new idea has been proposed in [70] for the solution of the local problems (4.5). It consists in *choosing the evaluation point* according to the *local geometry* and the *diffusion tensor*. The choice of the points $\mathbf{z}_K$ is done *locally* in order to: a) *ensure the well-posedness* of the *local problems* (4.5); b) *influence the properties* of the *local matrices* $\mathbb{M}_V$; c) *influence the properties* of the *final global system matrices* (see Sections 4.4.1
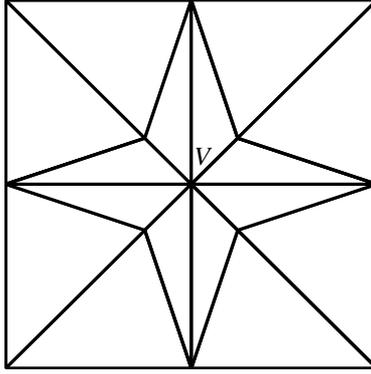
14

Figure 9: An example of a patch $\mathcal{T}_V$ where the matrix $\mathbb{M}_V$ is singular with barycenters as the evaluation points

and 4.4.2 below). We refer to [70] for the analysis of this approach. Proceeding as in this section, one the hope is to combine the advantages of Sections 4.1.1 and 4.1.2; in particular, one can arrive on local systems which are well-posed for any local geometry and tensor **S** (recall that this is not possible by any of the approaches of Sections 4.1.1 and 4.1.2). The numerical experiments of Section 6 below show that choosing the evaluation point can also lead to the superiority of this approach over the other ones in terms of computational properties.

4.2 Local problems definition by an algebraic interpretation

The approaches of Sections 4.1.1–4.1.3 all rely on the *geometrical interpretation* of the new unknown potential values $\bar{p}_K$ as the values of the Crouzeix–Raviart approximation $\tilde{\lambda}_h$ in the points $\mathbf{z}_K$. Following [70], it turns out that such a physical interpretation is not necessary and we can merely introduce a new unknown value $\bar{p}_K$ for each $K \in \mathcal{T}_h$ and relate it *algebraically* to the Lagrange multipliers λ_σ.

4.2.1 A general algebraic principle—potentials

Let $K \in \mathcal{T}_h$ and let $\Lambda_K = \{\lambda_\gamma\}_{\gamma \in \mathcal{E}_K^{\text{int}}}$ be the vector (of size $(d+1)$ for elements K in the interior of Ω) of the Lagrange multipliers associated with the sides of the element K. Then we set

$$\mathbb{N}_K \Lambda_K = \bar{p}_K, \tag{4.8}$$

where $\mathbb{N}_K$ is a $1 \times |\mathcal{E}_K^{\text{int}}|$ matrix, to be specified. In order to proceed further later on, we will also need the matrix $\mathbb{N}$ of size $|\mathcal{T}_h| \times |\mathcal{E}_h^{\text{int}}|$ whose rows are formed by the element matrices $\mathbb{N}_K$. Then the relation (4.8), for all $K \in \mathcal{T}_h$, can be written as

$$\mathbb{N}\Lambda = \bar{P}. \tag{4.9}$$

The approaches of Sections 4.1.1–4.1.3 have as entries of the matrix $\mathbb{N}_K$ the values of the basis functions at the evaluation point $\mathbf{z}_K$. Consequently,

$$\sum_{\sigma \in \mathcal{E}_K} (\mathbb{N}_K)_\sigma = 1 \tag{4.10}$$

holds true for all elements K in the interior of $\mathcal{T}_h$. As an example, the approach of Section 4.1.2 consists in taking all entries of $\mathbb{N}_K$ equal to $1/(d+1)$ for all interior elements K. The matrix $\mathbb{N}_K$

for the approach of Section 4.1.1 is specified in [71, equation (30)]. The generality of the approach of this section/of [70] lies in the fact that the condition (4.10) is not required.

Now consider a vertex $V \in \mathcal{V}_h$ and the lines in (1.6) associated with all interior sides of the patch $\mathcal{T}_V$, $\gamma \in \mathcal{E}_V^{\text{int}}$. Setting $\Lambda_V := \{\lambda_\gamma\}_{\gamma \in \mathcal{E}_V}$, $E_V^{\text{int}} := E_{\gamma \in \mathcal{E}_V^{\text{int}}}$, and denoting $\mathbb{Z}_V$ the corresponding submatrix of $\mathbb{Z}$, this gives

$$\mathbb{Z}_V \Lambda_V = E_V^{\text{int}}. \tag{4.11}$$

Equation (4.11) represents a rectangular linear system, where the number of equations (rows) is given by $|\mathcal{E}_V^{\text{int}}|$, the number of sides from $\mathcal{E}_h^{\text{int}}$ (the interior sides of $\mathcal{T}_h$) having V as vertex, and where the number of unknowns (columns) is given by $|\mathcal{E}_V|$, all the sides of the elements in $\mathcal{T}_V$ contained in $\mathcal{E}_h^{\text{int}}$. For an interior vertex V, we refer to Figure 4 for an illustration of these different sets. Now consider (4.8) on all elements $K \in \mathcal{T}_V$. This gives $|\mathcal{T}_V|$ (the number of elements in $\mathcal{T}_V$) equations for the unknowns Λ_V, expressed as a function of $\bar{P}_V$. Combing (4.8) on all elements $K \in \mathcal{T}_V$ and (4.11) gives altogether $|\mathcal{T}_V| + |\mathcal{E}_V^{\text{int}}|$ equations for the unknowns Λ_V (whose number is $|\mathcal{T}_V| + |\mathcal{E}_V^{\text{int}}|$), expressed as a function of $\bar{P}_V$ and E_V^{int}. We can write this algebraically as

$$\begin{pmatrix} \mathbb{Z}_V \\ \mathbb{N}_V \end{pmatrix} \Lambda_V = \begin{pmatrix} E_V^{\text{int}} \\ \bar{P}_V \end{pmatrix}. \tag{4.12}$$

We remark here that $|\mathcal{E}_V^{\text{ext}}| = |\mathcal{T}_V|$, except of the non interesting cases where $\mathcal{T}_h$ only has a couple of elements. Remark also that (4.11) represents a set of $|\mathcal{E}_V^{\text{int}}|$ linearly independent equations (as these equations are lines of the well-posed system (1.6)). Thus the well-posedness of (4.12) only depends on the matrix $\mathbb{N}_V$ given by the element matrices $\mathbb{N}_K$. Clearly, as in Section 4.1.3, but still in a more general fashion, the well-posedness of (4.12) can be controlled in function of the local constellation (local geometry, local values of $\mathbf{S}$) through the choice of the matrices $\mathbb{N}_K$, that we have entirely under our control. This is the subject of the study in [70]. Remark finally that (4.6) is a particular consequence of (4.12) when (4.10) holds true.

4.2.2 A general algebraic principle—fluxes

We have discussed in Section 4.1, recall (4.2), that whenever we can obtain local expressions of the Lagrange multipliers λ_γ inside (or in) the patch $\mathcal{T}_V$ as a function of the new element values $\bar{p}_K$ in the patch $\mathcal{T}_V$, we can also obtain the fluxes $\mathbf{u}_h$ in the whole patch $\mathcal{T}_V$ as a function of $\bar{p}_K$. Starting from the hybridized formulation (1.5) instead of (1.6) and following the same general idea as in Section 4.2.1, this can also be seen as follows: consider a vertex $V \in \mathcal{V}_h$ and the lines in (1.5) associated with all the elements of the patch $\mathcal{T}_V$ and their sides for the first block row, all the elements of the patch $\mathcal{T}_V$ for the second block row, and all the interior sides of the patch $\mathcal{T}_V$ for the last block row. Set U_V for all the elements of the patch $\mathcal{T}_V$ and their sides, P_V for all the elements of the patch $\mathcal{T}_V$, and Λ_V for the sides from $\mathcal{E}_V$. This gives the following local rectangular linear system:

$$\begin{pmatrix} \mathbb{A}_V & \mathbb{B}_V^t & \mathbb{C}_V^t \\ \mathbb{B}_V & 0 & 0 \\ \mathbb{C}_V & 0 & 0 \end{pmatrix} \begin{pmatrix} U_V \\ P_V \\ \Lambda_V \end{pmatrix} = \begin{pmatrix} F_V \\ G_V \\ 0_V \end{pmatrix}. \tag{4.13}$$

Combing (4.8) on all elements $K \in \mathcal{T}_V$ with (4.13) gives a local square linear system (with $(d+1)|\mathcal{T}_V| + |\mathcal{T}_V| + |\mathcal{E}_V^{\text{int}}| + |\mathcal{T}_V|$ equations and unknowns)

$$\begin{pmatrix} \mathbb{A}_V & \mathbb{B}_V^t & \mathbb{C}_V^t \\ \mathbb{B}_V & 0 & 0 \\ \mathbb{C}_V & 0 & 0 \\ 0 & 0 & \mathbb{N}_V \end{pmatrix} \begin{pmatrix} U_V \\ P_V \\ \Lambda_V \end{pmatrix} = \begin{pmatrix} F_V \\ G_V \\ 0_V \\ \bar{P}_V \end{pmatrix}. \tag{4.14}$$

The same comments as in Section 4.2.1 hold here true as well.

4.3 Expressing the Lagrange multipliers Λ and the fluxes U as a function of the potentials $\bar{P}$

Let $V \in \mathcal{V}_h$ be a vertex and $\mathcal{T}_V$ the corresponding patch. By any of the approaches of Sections 4.1–4.2, if the corresponding local problems (4.6), (4.12), or (4.14) are well-posed, we obtain local expressions of the Lagrange multipliers Λ_V^{int} (Λ_V) and/or local expressions of the fluxes U_V from the potentials $\bar{P}_V$ (and sources in $\mathcal{T}_V$). We in particular infer from (4.6)

$$\Lambda_V^{\mathrm{int}} = (\mathbb{M}_V)^{-1}(\widetilde{G}_V - \mathbb{J}_V \bar{P}_V) \tag{4.15}$$

and from (4.12)

$$\Lambda_V = \left(\begin{array}{c} \mathbb{Z}_V \\ \mathbb{N}_V \end{array} \right)^{-1} \left(\begin{array}{c} E_V^{\mathrm{int}} \\ \bar{P}_V \end{array} \right). \tag{4.16}$$

A similar expression can be obtained for U_V from all (4.6), (4.12), or (4.14).

We will now run through all vertices of the mesh $\mathcal{T}_h$. For every vertex V, we have one expression for Λ_V^{int}. Once the new potentials $\bar{P}$ are known, these different expressions have to lead to the same values of the Lagrange multipliers Λ. Thus, we are free to associate a *weight* $w_{V,\sigma}$ to the expression of Λ_σ from every patch $\mathcal{T}_V$ where the side σ is such that Λ_σ is the unknown in the local problem, and combine these expressions with these weights. The only (natural) condition is that, for every side σ, the sum of all its weights is equal to one. Let $V \in \mathcal{V}_h$. Let us define a mapping $\Upsilon_V : \mathbb{R}^{|\mathcal{E}_V^{\mathrm{int}}|} \to \mathbb{R}^{|\mathcal{E}_h^{\mathrm{int}}|}$, extending a vector $\Lambda_V^{\mathrm{int}} = \{\Lambda_\sigma\}_{\sigma \in \mathcal{E}_V^{\mathrm{int}}}$ of values associated with the sides from $\mathcal{E}_V^{\mathrm{int}}$ to a vector of values associated with all the interior sides $\mathcal{E}_h^{\mathrm{int}}$ by

$$[\Upsilon_V(\Lambda_V^{\mathrm{int}})]_\sigma := \left\{ \begin{array}{ll} \Lambda_\sigma & \text{if } \sigma \in \mathcal{E}_V^{\mathrm{int}} \\ 0 & \text{if } \sigma \notin \mathcal{E}_V^{\mathrm{int}} \end{array} \right. .$$

Let next $\mathbb{W}_V$ be a diagonal matrix of size $|\mathcal{E}_V^{\mathrm{int}}| \times |\mathcal{E}_V^{\mathrm{int}}|$, with the entries given by the weights $w_{V,\sigma}$. With these notations and assumptions, we have

$$\sum_{V \in \mathcal{V}_h} \Upsilon_V(\mathbb{W}_V \Lambda_V^{\mathrm{int}}) = \Lambda. \tag{4.17}$$

Let us now introduce a mapping $\Upsilon_V : \mathbb{R}^{|\mathcal{E}_V^{\mathrm{int}}| \times |\mathcal{E}_V^{\mathrm{int}}|} \to \mathbb{R}^{|\mathcal{E}_h^{\mathrm{int}}| \times |\mathcal{E}_h^{\mathrm{int}}|}$ (with the same name as the previous one, since there is no possibility of confusion), extending a local matrix $\mathbb{M}_V$ to a full-size one by zeros by

$$[\Upsilon_V(\mathbb{M}_V)]_{\sigma,\gamma} := \left\{ \begin{array}{ll} (\mathbb{M}_V)_{\sigma,\gamma} & \text{if } \sigma \in \mathcal{E}_V^{\mathrm{int}} \text{ and } \gamma \in \mathcal{E}_V^{\mathrm{int}} \\ 0 & \text{if } \sigma \notin \mathcal{E}_V^{\mathrm{int}} \text{ or } \gamma \notin \mathcal{E}_V^{\mathrm{int}} \end{array} \right. .$$

We finally in the same fashion define a mapping $\Theta_V : \mathbb{R}^{|\mathcal{E}_V^{\mathrm{int}}| \times |\mathcal{T}_V|} \to \mathbb{R}^{|\mathcal{E}_h^{\mathrm{int}}| \times |\mathcal{T}_h|}$, filling a full-size representation of a matrix $\mathbb{J}_V$ by zeros on the rows associated with the sides that are not from $\mathcal{E}_V^{\mathrm{int}}$ and on the columns associated with the elements that are not from $\mathcal{T}_V$,

$$[\Theta_V(\mathbb{J}_V)]_{\sigma,K} := \left\{ \begin{array}{ll} (\mathbb{J}_V)_{\sigma,K} & \text{if } \sigma \in \mathcal{E}_V^{\mathrm{int}} \text{ and } K \in \mathcal{T}_V \\ 0 & \text{if } \sigma \notin \mathcal{E}_V^{\mathrm{int}} \text{ or } K \notin \mathcal{T}_V \end{array} \right. .$$

With these notations, we obtain from (4.15)

$$\begin{aligned} \Upsilon_V(\mathbb{W}_V \Lambda_V^{\mathrm{int}}) &= \Upsilon_V(\mathbb{W}_V(\mathbb{M}_V)^{-1}(\widetilde{G}_V - \mathbb{J}_V \bar{P}_V)) \\ &= \Upsilon_V(\mathbb{W}_V(\mathbb{M}_V)^{-1})\widetilde{G} - \Theta_V(\mathbb{W}_V(\mathbb{M}_V)^{-1}\mathbb{J}_V)\bar{P}. \end{aligned}$$

17

Now, employing (4.17), we finally come to

$$\Lambda = \widetilde{\mathbb{M}}^{\mathrm{inv}} \widetilde{G} - \mathbb{M}^{\mathrm{inv}} \bar{P} \tag{4.18}$$

with

$$\widetilde{\mathbb{M}}^{\mathrm{inv}} := \sum_{V \in \mathcal{V}_h} \Upsilon_V (\mathbb{W}_V (\mathbb{M}_V)^{-1}), \quad \mathbb{M}^{\mathrm{inv}} := \sum_{V \in \mathcal{V}_h} \Theta_V (\mathbb{W}_V (\mathbb{M}_V)^{-1} \mathbb{J}_V).$$

A similar procedure as above can be applied for the local problems (4.12) or (4.14).

In the same way, in all (4.6), (4.12), or (4.14), also the fluxes can be expressed. We then arrive at the equivalent of (4.18) in the form

$$U = \widetilde{\mathbb{O}}^{\mathrm{inv}} G - \mathbb{O}^{\mathrm{inv}} \bar{P}. \tag{4.19}$$

Let us stress that all $\mathbb{M}^{\mathrm{inv}}$, $\widetilde{\mathbb{M}}^{\mathrm{inv}}$, $\mathbb{O}^{\mathrm{inv}}$, and $\widetilde{\mathbb{O}}^{\mathrm{inv}}$ are *fully computable* and *sparse matrices*, obtained by a weighted combination of the inverses of the local matrices. We would finally like to mention here that in the numerical experiments of Section 6, we only use the approach of Section 4.1. We set there all the weights $w_{V,\sigma}$ equal to $1/d$.

4.4 Prescribing the final system for the potentials $\bar{P}$ only

We now want to use the above developments in order to write a global system of the form (1.10). It turns out that two different approaches may be taken. In both of them, somehow surprisingly and unusually, we are going to *reuse the same equations* that have been previously used to obtain (4.18) or (4.19).

4.4.1 Prescribing the final system by an equilibrium of the fluxes

Using (4.19), the first way of writing a final linear system for the unknowns $\bar{P}$ only is to insert this expression into the second block equation of (1.3), i.e., into

$$\mathbb{B} U = G.$$

This gives

$$- \mathbb{B} \mathbb{O}^{\mathrm{inv}} \bar{P} = G - \mathbb{B} \widetilde{\mathbb{O}}^{\mathrm{inv}} G, \tag{4.20}$$

i.e., (1.10) with $\bar{\mathbb{S}} = -\mathbb{B} \mathbb{O}^{\mathrm{inv}}$ and $\bar{H} = G - \mathbb{B} \widetilde{\mathbb{O}}^{\mathrm{inv}} G$. Remark that here, the second block equation of (1.3) ($\mathbb{B} U = G$) is used in (4.6) (it is employed in (4.4))/in (4.14), as well as in (4.20). We now comment on the different approaches of Sections 4.1.1–4.1.3 when they are used in connection with (4.20).

In the approach of Section 4.1.1 (when it is feasible), following [72, 24, 71], the final matrix $\bar{\mathbb{S}}$ is *symmetric* and has a $(d+2)$-*point stencil* (there are at most $d+2$ nonzero entries per each row of $\bar{\mathbb{S}}$) (for each $K \in \mathcal{T}_h$, only its neighbors are involved). When $\mathbf{S}_K = \mathbb{I} s_K$, $\bar{\mathbb{S}}$ is *positive definite* on strictly Delaunay meshes but *indefinite* otherwise. A critical situation arises, as outlined in Section 4.1.1, in two space dimensions, when two triangles cut a square, see Figure 8. The local matrices $\mathbb{M}_V$ degenerate and the final problem (4.20) is *not well-posed*. In order to proceed, an "aggregation" of the two triangles into a square has to be done, leading to one final unknown for each aggregated pair of triangles. We refer for a detailed description of all these results and for further results to [72, 24, 71]. This approach is called in Section 6 below the FV method.

In the approach of Section 4.1.2, the final matrix $\bar{\mathbb{S}}$ is in general *nonsymmetric* and has a *wider stencil* (for each $K \in \mathcal{T}_h$, all simplices sharing a node with K are involved). The family of meshes

where $\bar{\mathbb{S}}$ is *positive definite* (which implies well-posedness) is, however, wider in comparison with the previous case. Recall that, similarly as in the previous case, *singular local matrices* $\mathbb{M}_V$ can appear, see Section 4.1.2. We refer for a detailed description of all these results and further results to [64]. This approach is called in Section 6 below the CMFE method.

Finally, the approach of Section 4.1.3 can be described similarly as that of Section 4.1.2.

4.4.2 Prescribing the final system by a potential relation

Using (4.18), the second way of writing a final linear system for the unknowns $\bar{P}$ only is to insert this expression into (4.9), i.e., into

$$\mathbb{N}\Lambda = \bar{P}.$$

This gives

$$\mathbb{N}\mathbb{M}^{\text{inv}}\bar{P} + \bar{P} = \mathbb{N}\widetilde{\mathbb{M}}^{\text{inv}}\widetilde{G}, \tag{4.21}$$

i.e., (1.10) with $\bar{\mathbb{S}} = \mathbb{N}\mathbb{M}^{\text{inv}} + \mathbb{I}$ and $\bar{H} = \mathbb{N}\widetilde{\mathbb{M}}^{\text{inv}}\widetilde{G}$. Remark that here, (4.9) is used repeatedly.

This approach is studied in detail in [70]. It turns out that the approach of Section 4.1.1, in contrast to Section 4.4.1, leads here in general to a *nonsymmetric* matrix. This approach is called in Section 6 below the MFEC method. The other approaches still lead to a *nonsymmetric* matrix as in Section 4.4.1. The *stencil* involves only neighbors of a given $K \in \mathcal{T}_h$ for Section 4.1.1 and all simplices sharing a node with a given $K \in \mathcal{T}_h$ in the other cases. *Positive definiteness* and *well-posedness* depend again on the mesh $\mathcal{T}_h$ and the diffusion tensor $\mathbf{S}$. The approaches of Sections 4.1.2 and 4.1.3, respectively, are called the MFEB and MFEO methods in Section 6 below.

4.5 Additional symmetry and positive definiteness issues

As we have described, the final matrix $\bar{\mathbb{S}}$ of (1.10), given by (4.20) or by (4.21), is generally nonsymmetric. The exception is the use of the $\mathbf{S}$-circumcenter as the geometric evaluation point of Section 4.1.1, while imposing the final system through (4.20).

Consider the case $\mathbf{S} = \mathbb{I}$ and the approach of Section 4.1.1 ($\mathbf{S}$-circumcenter as the geometric evaluation point), in combination with (4.21). It is observed in numerical experiments in [70] that in this case, the final matrix $\bar{\mathbb{S}}$ is symmetric if the mesh is "symmetric", consisting of the elements with the same shape, repeated in the mesh. Here the two approaches of imposing (1.10) through (4.20) or through (4.21) coincide. Interestingly enough, this is no more the case for an inhomogeneous or anisotropic diffusion tensor $\mathbf{S}$.

An open question that we find interesting is whether by adopting one of the approaches of Sections 4.1.3, 4.2.1, or 4.2.2 in combination with the use of the weights $w_{V,\sigma}$ of Section 4.3, we can obtain a symmetric and positive definite matrix for any mesh $\mathcal{T}_h$ and any diffusion tensor $\mathbf{S}$, either while imposing the final system as in Section 4.4.1, or as in Section 4.4.2.

5 Mixed finite elements on general polygonal meshes and their relations to other locally conservative methods

The aim of this section is to recall that mixed finite elements (of arbitrary order) can be used on general polygonal meshes $\widehat{\mathcal{T}}_H$ described in Section 1 in order to produce a scheme of the type (1.12) or (1.13).

Theorem 5.1 (Mixed finite elements on polygonal meshes under the form (1.13)). *Let $\widehat{\mathcal{T}}_H$ be an arbitrary polygonal mesh with a matching simplicial submesh $\mathcal{T}_h$. Consider any mixed finite*

element scheme on $\mathcal{T}_h$ leading to (1.6). *Then,* (1.6) *can be statically condensed into a well-posed system of the form* (1.13) *with a sparse, symmetric, and positive definite matrix* $\widehat{\mathbb{Z}}$.

Proof. Let a $K \in \widehat{\mathcal{T}}_H$ be given and denote the unknowns Λ of (1.6) corresponding to the sides of $\mathcal{T}_h$ which are in the interior of K by Λ_K^{int}. Use a similar notation E_K^{int} for the right-hand side entries of (1.6). Finally, denote the unknowns corresponding to sides of $\mathcal{T}_h$ which are on the boundary of K but not on the boundary of Ω by Λ_K^{ext}. Consider the lines of (1.6) associated with such sides of $\mathcal{T}_h$ which are in the interior of K. This gives rise to the following local problem:

$$\mathbb{Z}_K^{\mathrm{int}} \Lambda_K^{\mathrm{int}} = E_K^{\mathrm{int}} - \mathbb{Z}_K^{\mathrm{ext}} \Lambda_K^{\mathrm{ext}}. \tag{5.1}$$

Note that the system matrix $\mathbb{Z}_K^{\mathrm{int}}$ is square, *symmetric*, and *positive definite*, which implies the *well-posedness* of the local problem ($\mathbb{Z}_K^{\mathrm{int}}$ is a submatrix of $\mathbb{Z}$ corresponding to the lines and columns corresponding to the sides of $\mathcal{T}_h$ which are in the interior of K). Note also that (5.1) is a *local Dirichlet problem*, which allows to compute Λ_K^{int} from Λ_K^{ext} and E_K^{int}. More precisely, we have

$$\Lambda_K^{\mathrm{int}} = (\mathbb{Z}_K^{\mathrm{int}})^{-1}(E_K^{\mathrm{int}} - \mathbb{Z}_K^{\mathrm{ext}} \Lambda_K^{\mathrm{ext}}). \tag{5.2}$$

We now repeat the above procedure for all $K \in \widehat{\mathcal{T}}_H$. We finally use the lines of (1.6) associated with the sides of $\mathcal{T}_h$ which are on the boundary of some $K \in \widehat{\mathcal{T}}_H$ but not on the boundary of Ω, where we insert the expressions (5.2). This gives (1.13). Note that, contrarily to Section 4, *all equations* of (1.6) are *used exactly once*; this process is called *static condensation* and clearly leads to the well-posedness of (1.13) with $\widehat{\mathbb{Z}}$ being sparse, symmetric, and positive definite. □

Theorem 5.2 (Mixed finite elements on polygonal meshes under the form (1.12))**.** *Let $\widehat{\mathcal{T}}_H$ be an arbitrary polygonal mesh with a matching simplicial submesh $\mathcal{T}_h$. Consider any mixed finite element scheme on $\mathcal{T}_h$ leading to* (1.3). *Then,* (1.3) *can be statically condensed into a well-posed system of the form* (1.12) *of indefinite, saddle point type, with $\widehat{\mathbb{A}}$ being symmetric and $\widehat{\mathbb{B}}$ having full row rank.*

Proof. Consider such basis of the space Φ_h which contains the indicator functions ϕ_K of all $K \in \widehat{\mathcal{T}}_H$, i.e., the functions equal to one on K and zero elsewhere (then, all other basis functions of Φ_h have zero mean value on each $K \in \widehat{\mathcal{T}}_H$). Let a $K \in \widehat{\mathcal{T}}_H$ be given and consider the lines of the first block of (1.3), i.e., of $(\mathbb{A} \; \mathbb{B}^t)$, associated with such sides of $\mathcal{T}_h$ which are in the interior of K. Consider moreover the lines of the second block of (1.3), i.e., of $(\mathbb{B} \; 0)$, associated with all basis functions with support in K, other than ϕ_K. This gives rise to the following local problem:

$$\begin{pmatrix} \mathbb{A}_K^{\mathrm{int}} & (\mathbb{B}_K^0)^t \\ \mathbb{B}_K^0 & 0 \end{pmatrix} \begin{pmatrix} U_K^{\mathrm{int}} \\ P_K^0 \end{pmatrix} = \begin{pmatrix} F_K^{\mathrm{int}} - \mathbb{A}_K^{\mathrm{ext}} U_K^{\mathrm{ext}} \\ G_K^0 \end{pmatrix}. \tag{5.3}$$

The *well-posedness* of this local problem follows from the fact that it corresponds to a *local Neumann problem* with compatible data (the compatibility of the data follows from (1.3)). Using (5.3), we can compute the fluxes U_K^{int} and potentials P_K^0 in the interior of K as a function of the fluxes U_K^{ext} through the boundary of K. Note that the matrix of (5.3) is formed by lines and rows of the matrix of (1.3). It is now sufficient to insert these expressions for all $K \in \widehat{\mathcal{T}}_H$ into the remaining equations of (1.3), i.e., those associated with the lines of the first block of (1.3) associated with the sides of $\mathcal{T}_h$ which are on the boundary of some $K \in \widehat{\mathcal{T}}_H$ and those associated with the lines of the second block of (1.3) associated with the basis functions ϕ_K. This leads to a system of a form (1.12). Note that contrarily to Section 4, there is *no reuse of the same equations*. This procedure is called *static condensation* and clearly leads to the well-posedness and indefinite, saddle-point form of (1.12), with $\widehat{\mathbb{A}}$ being symmetric and $\widehat{\mathbb{B}}$ having full row rank. □
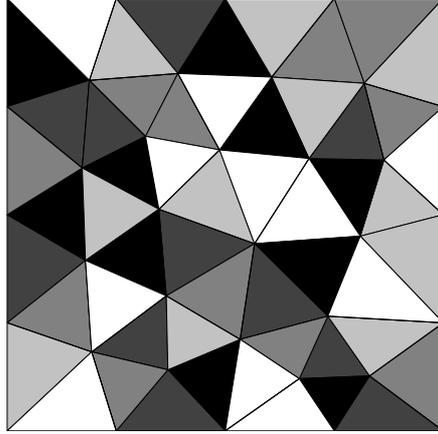
Figure 10: Initial mesh

Remark 5.3 (A priori and a posteriori error estimates)**.** *Using Theorems 5.1 and 5.2, (1.13) is only an algebraic rewriting of (1.6) and (1.12) is only an algebraic rewriting of (1.3). Thus, all a priori and a posteriori error estimates recalled in Section 1 are valid for mixed finite element methods also on arbitrary polygonal grids.*

Remark 5.4 (Discrete maximum principle on arbitrary polygonal meshes)**.** *In the same sense as in the previous remark, under the conditions discussed in Section 3.3, the discrete maximum principle is valid for mixed finite element methods also on arbitrary polygonal grids.*

6 Numerical experiments

The goal of this section is to carry out an extensive comparative numerical study of the different one-unknown-per-element reformulations of the lowest-order Raviart–Thomas mixed finite element method, as presented in Section 4. We study the behavior of the different approaches for the homogeneous and isotropic diffusion tensor in Section 6.1, for an anisotropic diffusion tensor in Section 6.2, and for an inhomogeneous diffusion tensor in Section 6.3.

We consider the problem (1.1a) on $\Omega = (0,1) \times (0,1)$, with inhomogeneous Dirichlet boundary condition given by the function $p(x,y) = 0.1y + 0.9$ instead of (1.1b). We perform the calculations on uniform refinements of the mesh viewed in Figure 10. This mesh is strictly Delaunay, with the minimal and maximal angles equal to 35.4 and 88.7 degrees, respectively. A sink term $g = -0.001$ is prescribed on two elements of the initial mesh. We consider the tensor $\mathbf{S}$ in the form

$$\mathbf{S}|_K = \begin{pmatrix} \cos(\theta_K) & -\sin(\theta_K) \\ \sin(\theta_K) & \cos(\theta_K) \end{pmatrix} \begin{pmatrix} s_K & 0 \\ 0 & \nu s_K \end{pmatrix} \begin{pmatrix} \cos(\theta_K) & \sin(\theta_K) \\ -\sin(\theta_K) & \cos(\theta_K) \end{pmatrix} \text{ for } K \in \mathcal{T}_h,$$

where we distinguish the following three different forms:

$$s_K = 1 \quad \forall K \in \mathcal{T}_h, \quad \nu = 1, \tag{6.1}$$

i.e. the homogeneous isotropic case ($\mathbf{S} = \mathbb{I}$), or

$$s_K = 1 \quad \forall K \in \mathcal{T}_h, \quad \theta_K \in \left\{ \frac{\pi}{5}, \frac{3\pi}{4}, \frac{\pi}{2}, \frac{3\pi}{5}, \frac{\pi}{3} \right\}, \quad \nu = 0.2, \tag{6.2}$$
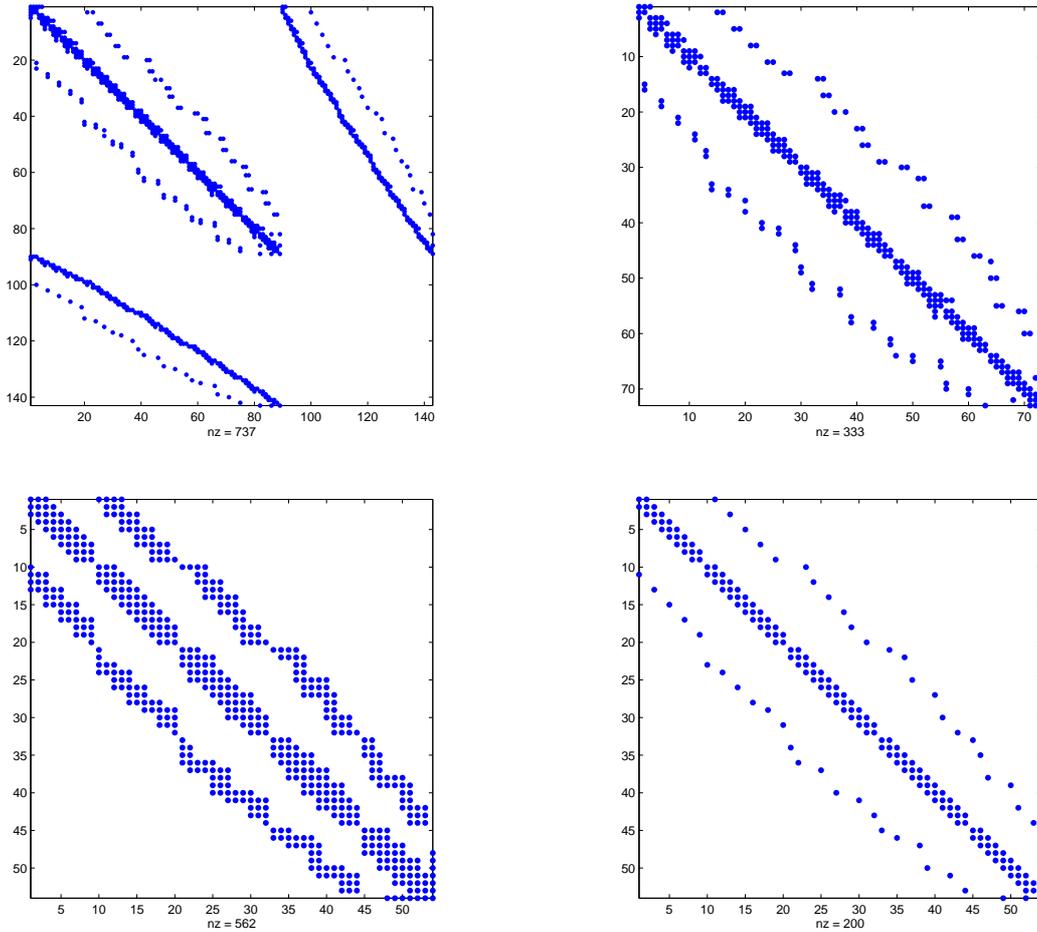
21

Figure 11: System matrix sparsity pattern of the original MFE formulation (top left), NCFE formulation (top right), MFEB, MFEO, and CMFE formulations (bottom left), and FV and MFEC formulations (bottom right) for the mesh of Figure 10

i.e. the (homogeneous with respect to s_K) anisotropic case ($\mathbf{S}$ is a full-matrix tensor), or

$$s_K \in \{10, 1, 0.1, 0.01, 0.001\}, \quad \nu = 1, \tag{6.3}$$

i.e. the inhomogeneous isotropic case ($\mathbf{S}$ is a varying multiple of the identity matrix). The different grey shades in Figure 10 correspond to the different choices θ_K and s_K in (6.2) and (6.3), respectively. All the computations were performed in double precision on a notebook with Intel Core2 Duo 2.6 GHz processor and MS Windows Vista operating system. Machine precision was in the power of 1e-16. All the linear system solutions were done with the help of MATLAB 7.0.4. Additional numerical experiments are presented in [70].

We test the following methods, which are all *equivalent implementations* of the lowest-order Raviart–Thomas mixed finite element method (1.2a)–(1.2b) (written as (1.3) in the matrix form):

1. **MFEB**: the final system is of the form (1.10), imposed through (4.21), with the barycenter as the evaluation point (cf. Section 4.1.2); this is the approach studied in [70];

2. **MFEC**: the final system is of the form (1.10), imposed through (4.21), with the $\mathbf{S}$-circum-center as the evaluation point (cf. Section 4.1.1); this is the approach studied in [70];

22

Abbreviation	Meaning
Meth.	method, one of the equivalent mixed finite element formulations
Un.	number of unknowns (matrix size)
Mat.	matrix
St.	stencil (the maximum number of nonzero entries on each matrix row)
Nonz.	total number of matrix nonzero entries
CN	2-norm condition number
CNS	2-norm condition number after diagonal scaling
DS	direct linear solver
CG	conjugate gradients iterative linear solver
PCG	preconditioned conjugate gradients iterative linear solver
Bi-CGStab	bi-conjugate gradients stabilized iterative linear solver
PBi-CGStab	preconditioned bi-conjugate gradients stabilized iterative linear solver
CPU	CPU time of a direct/iterative linear solver
Iter.	number of iterations of an iterative linear solver
IC	CPU time of incomplete Cholesky factorization with a specified drop tolerance
ILU	CPU time of incomplete LU factorization with a specified drop tolerance
SPD	symmetric positive definite
SID	symmetric indefinite
NPD	nonsymmetric positive definite
NNS	nonsymmetric negative stable
NID	nonsymmetric indefinite

Table 1: Abbreviations used in Tables 2–5

3. **MFEO**: the final system is of the form (1.10), imposed through (4.21), while choosing the evaluation point as a function of the local geometry (cf. Section 4.1.3); this is the approach studied in [70];

4. **CMFE**: the final system is of the form (1.11), given by the approach of [64]; considering the discrete unknowns $\bar{p}_K$ of (4.1) with the barycenter as the evaluation point (cf. Section 4.1.2) instead of p_K (recall the relation (3.4b)), the system matrix $\mathbb{S}$ of (1.11) is the same as the system matrix $\bar{\mathbb{S}}$ of (1.10) imposed through (4.20);

5. **FV**: the final system is of the form (1.10), imposed through (4.20), with the **S**-circumcenter as the evaluation point (cf. Section 4.1.1); this is the approach of [72, 24, 71] and corresponds to the finite volume method;

6. **NCFE**: the final system is of the form (1.6), imposed through (3.2), i.e., through the Crouzeix–Raviart nonconforming finite element method, see Section 3.1.

We show in Figure 11 the sparsity patterns of the original mixed finite element method (1.3) and of its equivalent reformulations of the above list, for the case of the mesh of Figure 10. In Tables 2–5, we present various properties of the final matrix systems arising from the different equivalent reformulations. We summarize in Table 1 the different abbreviations used in Tables 2–5. Recall that a real matrix $\mathbb{S} \in \mathbb{R}^{M \times M}$ is positive definite if $P^t \mathbb{S} P > 0$ for all $P \in \mathbb{R}^M$, $P \neq 0$, and negative stable when all its eigenvalues have positive real parts (this is in particular the case for positive

Meth.	Un.	Mat.	St.	Nonz.	CN	CNS	DS CPU	CG/ Bi-CGStab CPU	Iter.	PCG/ PBi-CGStab CPU	IC/ ILU	Iter.
MFEB	13824	NPD	14	177652	7564	7580	0.27	4.86	324.5	0.81	0.36	9.0
MFEC	13824	NNS	4	55040	11256	11056	0.09	2.23	372.0	0.42	0.19	6.5
MFEO	13824	NPD	14	177652	7531	7558	0.28	4.08	270.0	0.80	0.41	7.5
CMFE	13824	NPD	14	177652	7397	7380	0.27	4.70	312.0	0.83	0.39	8.5
FV	13824	SPD	4	55040	65722	8898	0.07	3.09	1098.0	0.42	0.17	17.0
NCFE	20608	SPD	5	102528	14064	9944	0.14	2.92	620.0	1.11	0.56	19.0

Table 2: Matrix properties and computational cost of the different equivalent equivalent formulations of the mixed finite element method, coefficients (6.1)

definite matrices). The 2-norm condition number of a matrix $\mathbb{S}$ is defined by $\|\mathbb{S}\|_2\|\mathbb{S}^{-1}\|_2$. We also consider the 2-norm condition number after diagonal scaling, by which we mean the minimal of the two 2-norm condition numbers of the two matrices

$$(\mathrm{diag}(\mathbb{S}))^{-1}\,\mathbb{S}, \quad |\mathrm{diag}(\mathbb{S})|^{-1/2}\,\mathbb{S}\,|\mathrm{diag}(\mathbb{S})|^{-1/2}.$$

We also study the computational cost. We first test the Matlab \ direct solver. A direct solver may not be usable for very large systems or may not be suitable for parabolic or nonlinear problems. Thus the behavior of iterative solvers is very important. We test two iterative methods. If the matrix is symmetric and positive definite, we use the conjugate gradients method [41, 56]. For nonsymmetric matrices, we employ the bi-conjugate gradients stabilized method [56, 63]. Unpreconditioned iterative linear solvers may be rather slow but usually illustrate well the matrix properties and especially the matrix condition number. To accelerate their convergence, we use incomplete Cholesky and incomplete LU factorizations with a specified drop tolerance, cf. [60]. The drop tolerance is always chosen in such a way that the sum of CPU times of the preconditioning and of the solution of the preconditioned system was minimal. We always use a zero start vector and stop the iterative process as soon as the relative residual $\|H - \mathbb{S}\tilde{P}\|_2/\|H\|_2$, where $\tilde{P}$ is the approximate solution to the system $\mathbb{S}P = H$, decreases below 1e-8.

Some general conclusions may be drawn from the theoretical investigations and from Tables 2–5. The number of unknowns is given by the number of elements for all methods except of NCFE, where the number of unknowns is given by the number of interior sides. NCFE always produces a symmetric positive definite matrix. The FV matrix is always symmetric, but positive definiteness depends on the tensor $\mathbf{S}$ and on the mesh $\mathcal{T}_h$. All the other methods lead to nonsymmetric matrices (see the discussion in Sections 4.4 and 4.5). These matrices can be positive definite, negative stable, or indefinite, in dependence on $\mathbf{S}$ and $\mathcal{T}_h$. Methods FV and MFEC produce four nonzero entries per matrix row in the interior of the mesh. In the NCFE case, this number is equal to 5. The stencil of the other methods is variable (recall that on the row associated with a given element K, there are nonzero entries on columns associated with those elements L which share a vertex with K); it the present case, this is equal to 14. Methods MFEC and FV lead to fewest total nonzero matrix entries; NCFE has roughly twice and the other methods have roughly three times as many nonzeros.

							DS	CG/ Bi-CGStab		PCG/ PBi-CGStab		
											IC/	
Meth.	Un.	Mat.	St.	Nonz.	CN	CNS	CPU	CPU	Iter.	CPU	ILU	Iter.
MFEB	55296	NPD	14	714740	30289	30373	1.51	33.31	530.0	8.14	3.37	19.5
MFEC	55296	NNS	4	220672	45016	44643	0.49	17.47	624.5	3.34	1.25	13.5
MFEO	55296	NPD	14	714740	30143	30285	1.55	37.76	594.5	7.06	2.75	19.5
CMFE	55296	NPD	14	714740	29630	29551	1.49	34.32	544.5	6.91	2.73	18.5
FV	55296	SPD	4	220672	263036	35813	0.48	29.52	2170.0	3.08	1.47	20.0
NCFE	82688	SPD	5	412416	56416	39901	0.90	35.80	1219.0	9.41	3.78	42.0

Table 3: Matrix properties and computational cost of the different equivalent equivalent formulations of the mixed finite element method, coefficients (6.1)

							DS	CG/ Bi-CGStab		PCG/ PBi-CGStab		
											IC/	
Meth.	Un.	Mat.	St.	Nonz.	CN	CNS	CPU	CPU	Iter.	CPU	ILU	Iter.
MFEB	13824	NPD	14	177652	14489	11203	0.28	6.61	448.0	0.98	0.59	6.5
MFEC	13824	NID	4	55040	2401279	416769	0.08	—	—	0.45	0.20	7.0
MFEO	13824	NPD	14	177652	13401	10767	0.27	6.51	440.5	0.95	0.41	10.0
CMFE	13824	NPD	14	177652	9276	7758	0.28	5.27	350.5	0.84	0.38	9.0
FV	13824	SID	4	55040	247055	239934	0.09	—	—	0.45	0.20	7.0
NCFE	20608	SPD	5	102528	25393	16969	0.18	4.03	850.0	1.12	0.41	30.0

Table 4: Matrix properties and computational cost of the different equivalent equivalent formulations of the mixed finite element method, coefficients (6.2)

6.1 Identity matrix diffusion tensor

Tables 2 and 3 present the results for the coefficients (6.1) and respectively fourth- and fifth-level uniform refinements of the mesh of Figure 10. The condition number of all methods is here roughly comparable; the only (negative) exception is the FV method. The condition numbers get mutually much closer after the diagonal scaling. The matrix size and sparsity pattern/number of nonzero entries imply that FV/MFEC give smallest CPU times while using the direct solver, followed respectively by NCFE and then all other methods. The method MFEC behaves best for an unpreconditioned linear solver, actually much better than FV which do has the advantage of a symmetric matrix. The methods MFEB/MFEC/MFEO proposed in the present paper and the related CMFE method seem to outperform NCFE for increasing mesh size (a systematically better behavior of CMFE over NCFE is observed in [64]). Concerning preconditioned iterative solvers, FV/MFEC seem to perform roughly two times as fast as MFEB/MFEO/CMFE and roughly three times as fast as NCFE.

| | | | | | | | DS | CG/ Bi-CGStab | | PCG/ PBi-CGStab | | |
| | | | | | | | | | | | IC/ | |
Meth.	Un.	Mat.	St.	Nonz.	CN	CNS	CPU	CPU	Iter.	CPU	ILU	Iter.
MFEB	13824	NPD	14	177652	819248	740706	0.28	13.33	897.5	1.05	0.62	6.5
MFEC	13824	NNS	4	55040	903789	763849	0.09	5.34	947.5	0.47	0.20	7.5
MFEO	13824	NPD	14	177652	820367	739957	0.28	12.45	790.5	1.05	0.56	8.0
CMFE	13824	NPD	14	177652	2500730	478974	0.28	102.27	6842.5	1.01	0.41	10.5
FV	13824	SPD	4	55040	16387758	497974	0.07	39.41	14101.0	0.44	0.17	16.0
NCFE	20608	SPD	5	102528	4797335	670623	0.18	52.42	11226.0	1.22	0.64	16.0

Table 5: Matrix properties and computational cost of the different equivalent equivalent formulations of the mixed finite element method, coefficients (6.3)

6.2 Anisotropic diffusion tensor

Table 4 presents the results for the coefficients (6.2) and the fourth-level uniform refinement of the mesh of Figure 10. Because of the anisotropy of the diffusion tensor, the FV method leads to a symmetric indefinite matrix, whereas the MFEC method to a nonsymmetric indefinite matrix. These matrices are also very badly conditioned, whereby the diagonal scaling does not help too much. Consequently, direct application of the iterative solvers leads to no convergence in 50000 iterations. All the other methods behave rather similarly to Table 2. Application of the direct solver or of iterative solvers with preconditioning leads to results similar to that of Table 2.

6.3 Inhomogeneous diffusion tensor

Table 5 presents the results for the coefficients (6.3) and the fourth-level uniform refinement of the mesh of Figure 10. Here the matrices are as for the identity matrix diffusion tensor of Tables 2 and 3; in particular the FV method gives a symmetric positive definite matrix and MFEC a nonsymmetric negative stable matrix. The inhomogeneity of the diffusion tensor however causes an increase of the matrices condition numbers. This increase is severe in CMFE and NCFE methods, and in particular in the FV method. Consequently, direct application of the iterative solvers leads to important increase of the CPU time in CMFE, NCFE, and FV methods. Whereas the FV and MFEC methods behaved similarly in Table 2, the MFEC method becomes here almost 8 times faster than the FV one. When diagonal scaling is applied, however, the condition numbers of all methods become comparable, whence the preconditioned iterative solvers behave similarly as for the case of Table 2. Also the application of the direct solver leads to results similar to those of Table 2.

7 Conclusions

We have introduced in this paper a systematic way of reducing the number of unknowns in the lowest-order Raviart–Thomas mixed finite element method from the flux and potential unknowns to (new) potential unknowns only. This gives rise to a whole family of equivalent one-unknown-per-element reformulations of the mixed finite element method, some of which reduce to some well-known discretization schemes. Amongst these equivalent formulations, the MFEC leads to very

compact 4-point stencils in two space dimensions and excellent computational costs for problems with a possibly highly inhomogeneous diffusion tensor. The FV has similar properties and leads, in addition, to symmetric matrices, but behaves considerably worse for highly inhomogeneous diffusion tensors. Both of these reformulations, however, seem to behave less well for anisotropic diffusion tensors, and, moreover, are only applicable in two space dimensions. Then the MFEB, MFEO, or the previously proposed CMFE reformulations seem as appealing alternatives to the classical NCFE implementation.

We have also recalled the validity of the discrete maximum principle and the possibility to formulate mixed finite element methods on general polygonal meshes. To us, the major conclusion of the present paper is that in all underlying principles, derivation, properties, applicability, and computational cost, the lowest-order Raviart–Thomas mixed finite element method is closely related to many other locally conservative discretization methods, while possessing a well-explored and solid theoretical background.

References

[1] AAVATSMARK, I., BARKVE, T., BØE, Ø., AND MANNSETH, T. Discretization on unstructured grids for inhomogeneous, anisotropic media. I. Derivation of the methods. *SIAM J. Sci. Comput. 19*, 5 (1998), 1700–1716.

[2] AAVATSMARK, I., BARKVE, T., BØE, Ø., AND MANNSETH, T. Discretization on unstructured grids for inhomogeneous, anisotropic media. II. Discussion and numerical results. *SIAM J. Sci. Comput. 19*, 5 (1998), 1717–1736.

[3] AAVATSMARK, I., EIGESTAD, G. T., KLAUSEN, R. A., WHEELER, M. F., AND YOTOV, I. Convergence of a symmetric MPFA method on quadrilateral grids. *Comput. Geosci. 11*, 4 (2007), 333–345.

[4] AGÉLAS, L., DI PIETRO, D. A., AND DRONIOU, J. The G method for heterogeneous anisotropic diffusion on general meshes. *M2AN Math. Model. Numer. Anal. 44*, 4 (2010), 597–625.

[5] AGELAS, L., AND MASSON, R. Convergence of the finite volume MPFA O scheme for heterogeneous anisotropic diffusion problems on general meshes. *C. R. Math. Acad. Sci. Paris 346*, 17-18 (2008), 1007–1012.

[6] AGOUZAL, A., BARANGER, J., MAÎTRE, J.-F., AND OUDIN, F. Connection between finite volume and mixed finite element methods for a diffusion problem with nonconstant coefficients. Application to a convection diffusion problem. *East-West J. Numer. Math. 3*, 4 (1995), 237–254.

[7] AINSWORTH, M. A posteriori error estimation for lowest order Raviart–Thomas mixed finite elements. *SIAM J. Sci. Comput. 30*, 1 (2007), 189–204.

[8] ALOTTO, P., AND PERUGIA, I. Mixed finite element methods and tree-cotree implicit condensation. *Calcolo 36*, 4 (1999), 233–248.

[9] ARBOGAST, T., AND CHEN, Z. On the implementation of mixed methods as nonconforming methods for second-order elliptic problems. *Math. Comp. 64*, 211 (1995), 943–972.

[10] Arbogast, T., Dawson, C. N., Keenan, P. T., Wheeler, M. F., and Yotov, I. Enhanced cell-centered finite differences for elliptic equations on general geometry. *SIAM J. Sci. Comput. 19*, 2 (1998), 404–425.

[11] Arbogast, T., Pencheva, G., Wheeler, M. F., and Yotov, I. A multiscale mortar mixed finite element method. *Multiscale Model. Simul. 6*, 1 (2007), 319–346.

[12] Arbogast, T., Wheeler, M. F., and Yotov, I. Mixed finite elements for elliptic problems with tensor coefficients as cell-centered finite differences. *SIAM J. Numer. Anal. 34*, 2 (1997), 828–852.

[13] Arnold, D. N., and Brezzi, F. Mixed and nonconforming finite element methods: implementation, postprocessing and error estimates. *RAIRO Modél. Math. Anal. Numér. 19*, 1 (1985), 7–32.

[14] Baranger, J., Maître, J.-F., and Oudin, F. Connection between finite volume and mixed finite element methods. *RAIRO Modél. Math. Anal. Numér. 30*, 4 (1996), 445–465.

[15] Bause, M., Hoffmann, J., and Knabner, P. First-order convergence of multi-point flux approximation on triangular grids and comparison with mixed finite element methods. *Numer. Math. 116*, 1 (2010), 1–29.

[16] Becker, R., and Mao, S. An optimally convergent adaptive mixed finite element method. *Numer. Math. 111*, 1 (2008), 35–54.

[17] Breil, J., and Maire, P.-H. A cell-centered diffusion scheme on two-dimensional unstructured meshes. *J. Comput. Phys. 224*, 2 (2007), 785–823.

[18] Brenner, S. C. A multigrid algorithm for the lowest-order Raviart-Thomas mixed triangular finite element method. *SIAM J. Numer. Anal. 29*, 3 (1992), 647–678.

[19] Brezzi, F., and Fortin, M. *Mixed and hybrid finite element methods*, vol. 15 of *Springer Series in Computational Mathematics*. Springer-Verlag, New York, 1991.

[20] Brezzi, F., Lipnikov, K., and Shashkov, M. Convergence of the mimetic finite difference method for diffusion problems on polyhedral meshes. *SIAM J. Numer. Anal. 43*, 5 (2005), 1872–1896.

[21] Cancès, C., Gallouët, T., and Porretta, A. Two-phase flows involving capillary barriers in heterogeneous porous media. *Interfaces Free Bound. 11*, 2 (2009), 239–258.

[22] Cao, Y., Helmig, R., and Wohlmuth, B. I. Geometrical interpretation of the multi-point flux approximation L-method. *Internat. J. Numer. Methods Fluids 60*, 11 (2009), 1173–1199.

[23] Carstensen, C., and Hoppe, R. H. W. Error reduction and convergence for an adaptive mixed finite element method. *Math. Comp. 75*, 255 (2006), 1033–1042.

[24] Chavent, G., Younès, A., and Ackerer, P. On the finite volume reformulation of the mixed finite element method for elliptic and parabolic PDE on triangles. *Comput. Methods Appl. Mech. Engrg. 192*, 5-6 (2003), 655–682.

[25] Chen, L., Holst, M., and Xu, J. Convergence and optimality of adaptive mixed finite element methods. *Math. Comp. 78*, 265 (2009), 35–53.

[26] Chen, Z. Equivalence between and multigrid algorithms for nonconforming and mixed methods for second-order elliptic problems. *East-West J. Numer. Math. 4*, 1 (1996), 1–33.

[27] Ciarlet, P. G. *The Finite Element Method for Elliptic Problems*, vol. 4 of *Studies in Mathematics and its Applications*. North-Holland, Amsterdam, 1978.

[28] Cockburn, B., and Gopalakrishnan, J. A characterization of hybridized mixed methods for second order elliptic problems. *SIAM J. Numer. Anal. 42*, 1 (2004), 283–301.

[29] Cockburn, B., and Gopalakrishnan, J. Error analysis of variable degree mixed methods for elliptic problems via hybridization. *Math. Comp. 74*, 252 (2005), 1653–1677.

[30] Crouzeix, M., and Raviart, P.-A. Conforming and nonconforming finite element methods for solving the stationary Stokes equations. I. *Rev. Française Automat. Informat. Recherche Opérationnelle Sér. Rouge 7*, R-3 (1973), 33–75.

[31] Droniou, J., and Eymard, R. A mixed finite volume scheme for anisotropic diffusion problems on any grid. *Numer. Math. 105*, 1 (2006), 35–71.

[32] Droniou, J., Eymard, R., Gallouët, T., and Herbin, R. A unified approach to mimetic finite difference, hybrid finite volume and mixed finite volume methods. *Math. Models Methods Appl. Sci. 20*, 2 (2010). DOI 10.1142/S0218202510004222.

[33] Edwards, M. G. Unstructured, control-volume distributed, full-tensor finite-volume schemes with flow based grids. *Comput. Geosci. 6*, 3-4 (2002), 433–452. Locally conservative numerical methods for flow in porous media.

[34] Eymard, R., Gallouët, T., and Herbin, R. Finite volume methods. In *Handbook of Numerical Analysis, Vol. VII*. North-Holland, Amsterdam, 2000, pp. 713–1020.

[35] Eymard, R., Gallouët, T., and Herbin, R. Discretisation of heterogeneous and anisotropic diffusion problems on general non-conforming meshes, SUSHI: A scheme using stabilisation and hybrid interfaces. *IMA J. Numer. Anal.* (2010). DOI 10.1093/imanum/drn084.

[36] Eymard, R., Gallouët, T., Herbin, R., and Michel, A. Convergence of a finite volume scheme for nonlinear degenerate parabolic equations. *Numer. Math. 92*, 1 (2002), 41–82.

[37] Eymard, R., Herbin, R., and Michel, A. Mathematical study of a petroleum-engineering scheme. *M2AN Math. Model. Numer. Anal. 37*, 6 (2003), 937–972.

[38] Eymard, R., Hilhorst, D., and Vohralík, M. A combined finite volume–nonconforming/mixed-hybrid finite element scheme for degenerate parabolic problems. *Numer. Math. 105*, 1 (2006), 73–131.

[39] Glowinski, R., and Wheeler, M. F. Domain decomposition and mixed finite element methods for elliptic problems. In *First International Symposium on Domain Decomposition Methods for Partial Differential Equations (Paris, 1987)*. SIAM, Philadelphia, PA, 1988, pp. 144–172.

[40] Gyrya, V., and Lipnikov, K. High-order mimetic finite difference method for diffusion problems on polygonal meshes. *J. Comput. Phys. 227*, 20 (2008), 8841–8854.

[41] Hestenes, M. R., and Stiefel, E. Methods of conjugate gradients for solving linear systems. *J. Research Nat. Bur. Standards 49* (1952), 409–436 (1953).

[42] HOFFMANN, J. Equivalence of the lowest-order Raviart–Thomas mixed finite element method and the multi point flux approximation scheme on triangular grids. Preprint, University of Erlangen-Nürnberg, 2008.

[43] HYMAN, J., SHASHKOV, M., AND STEINBERG, S. The numerical solution of diffusion problems in strongly heterogeneous non-isotropic materials. *J. Comput. Phys. 132*, 1 (1997), 130–148.

[44] KLAUSEN, R. A., RADU, F. A., AND EIGESTAD, G. T. Convergence of MPFA on triangulations and for Richards' equation. *Internat. J. Numer. Methods Fluids 58*, 12 (2008), 1327–1351.

[45] KLAUSEN, R. A., AND RUSSELL, T. F. Relationships among some locally conservative discretization methods which handle discontinuous coefficients. *Comput. Geosci. 8*, 4 (2004), 341–377 (2005).

[46] KLAUSEN, R. A., AND WINTHER, R. Convergence of multipoint flux approximations on quadrilateral grids. *Numer. Methods Partial Differential Equations 22*, 6 (2006), 1438–1454.

[47] KUZNETSOV, Y. Mixed finite element methods for diffusion equations on nonmatching grids. In *Domain decomposition methods in science and engineering*, vol. 40 of *Lect. Notes Comput. Sci. Eng.* Springer, Berlin, 2005, pp. 311–318.

[48] KUZNETSOV, Y., AND REPIN, S. New mixed finite element method on polygonal and polyhedral meshes. *Russian J. Numer. Anal. Math. Modelling 18*, 3 (2003), 261–278.

[49] KUZNETSOV, Y., AND REPIN, S. Convergence analysis and error estimates for mixed finite element method on distorted meshes. *J. Numer. Math. 13*, 1 (2005), 33–51.

[50] KUZNETSOV, Y. A. Mixed finite element methods on polyhedral meshes for diffusion equations. In *Partial differential equations*, vol. 16 of *Comput. Methods Appl. Sci.* Springer, Dordrecht, 2008, pp. 27–41.

[51] LE POTIER, C. Schéma volumes finis pour des opérateurs de diffusion fortement anisotropes sur des maillages non structurés. *C. R. Math. Acad. Sci. Paris 340*, 12 (2005), 921–926.

[52] LIPNIKOV, K., SHASHKOV, M., AND YOTOV, I. Local flux mimetic finite difference methods. *Numer. Math. 112*, 1 (2009), 115–152.

[53] MAÎTRE, J.-F. personnal communication. 2004.

[54] MARINI, L. D. An inexpensive method for the evaluation of the solution of the lowest order Raviart–Thomas mixed method. *SIAM J. Numer. Anal. 22*, 3 (1985), 493–496.

[55] NÉDÉLEC, J.-C. Mixed finite elements in $\mathbb{R}^3$. *Numer. Math. 35*, 3 (1980), 315–341.

[56] QUARTERONI, A., AND VALLI, A. *Numerical approximation of partial differential equations*, vol. 23 of *Springer Series in Computational Mathematics*. Springer-Verlag, Berlin, 1994.

[57] RAVIART, P.-A., AND THOMAS, J.-M. A mixed finite element method for 2nd order elliptic problems. In *Mathematical aspects of finite element methods (Proc. Conf., Consiglio Naz. delle Ricerche (C.N.R.), Rome, 1975)*. Springer, Berlin, 1977, pp. 292–315. Lecture Notes in Math., Vol. 606.

[58] ROBERTS, J. E., AND THOMAS, J.-M. Mixed and hybrid methods. In *Handbook of Numerical Analysis, Vol. II.* North-Holland, Amsterdam, 1991, pp. 523–639.

[59] RUSSELL, T. F., AND WHEELER, M. F. Finite element and finite difference methods for continuous flows in porous media. In *The Mathematics of Reservoir Simulation.* SIAM, Philadelphia, 1983, pp. 35–106.

[60] SAAD, Y. *Iterative methods for sparse linear systems*, second ed. Society for Industrial and Applied Mathematics, Philadelphia, PA, 2003.

[61] SBOUI, A., JAFFRÉ, J., AND ROBERTS, J. A composite mixed finite element for hexahedral grids. *SIAM J. Sci. Comput. 31*, 4 (2009), 2623–2645.

[62] SCHEICHL, R. Decoupling three-dimensional mixed problems using divergence-free finite elements. *SIAM J. Sci. Comput. 23*, 5 (2002), 1752–1776.

[63] VAN DER VORST, H. A. Bi-CGSTAB: a fast and smoothly converging variant of Bi-CG for the solution of nonsymmetric linear systems. *SIAM J. Sci. Statist. Comput. 13*, 2 (1992), 631–644.

[64] VOHRALÍK, M. Equivalence between lowest-order mixed finite element and multi-point finite volume methods on simplicial meshes. *M2AN Math. Model. Numer. Anal. 40*, 2 (2006), 367–391.

[65] VOHRALÍK, M. A posteriori error estimates for lowest-order mixed finite element discretizations of convection-diffusion-reaction equations. *SIAM J. Numer. Anal. 45*, 4 (2007), 1570–1599.

[66] VOHRALÍK, M. Unified primal formulation-based a priori and a posteriori error analysis of mixed finite element methods. *Math. Comp. 79*, 272 (2010), 2001–2032.

[67] VOHRALÍK, M., MARYŠKA, J., AND SEVERÝN, O. Mixed and nonconforming finite element methods on a system of polygons. *Appl. Numer. Math. 57* (2007), 176–193.

[68] WHEELER, M. F., AND YOTOV, I. A multipoint flux mixed finite element method. *SIAM J. Numer. Anal. 44*, 5 (2006), 2082–2106.

[69] WOHLMUTH, B. I., AND VOHRALÍK, M. All order mixed finite element methods with one unknown per element. In preparation, 2010.

[70] WOHLMUTH, B. I., AND VOHRALÍK, M. A general principle for reducing the number of unknowns and influencing the matrix properties in nonconforming finite elements. In preparation, 2010.

[71] YOUNÈS, A., ACKERER, P., AND CHAVENT, G. From mixed finite elements to finite volumes for elliptic PDEs in two and three dimensions. *Internat. J. Numer. Methods Engrg. 59*, 3 (2004), 365–388.

[72] YOUNÈS, A., MOSE, R., ACKERER, P., AND CHAVENT, G. A new formulation of the mixed finite element method for solving elliptic and parabolic PDE with triangular elements. *J. Comput. Phys. 149*, 1 (1999), 148–167.